이학박사 학위논문

Controlled Organization of Colloidal Nanomaterials with Block Copolymer Micelles

블록공중합체 마이셀을 이용한 콜로이드 나노소재 조립 및 배열 제어

2015 년 2 월

서울대학교 대학원

화학부 고분자화학

김 정 희

Controlled Organization of Colloidal Nanomaterials with Block Copolymer Micelles

지도 교수 손 병 혁

이 논문을 이학박사 학위논문으로 제출함
2014 년 12 월

서울대학교 대학원
화학부 고분자화학
김 정 희

김정희의 이학박사 학위논문을 인준함
2014 년 12 월

위 원 장 이 진 규 (인)

부위원장 손 병 혁 (인)

위 원 정 택 동 (인)

위 원 최 태 림 (인)

위 원 송 오 성 (인)

Abstract

Controlled Organization of Colloidal Nanomaterials with Block Copolymer Micelles

Jeong-Hee Kim

Department of Chemistry

The Graduate School

Seoul National University

Colloidal nanoparticles based on organic and inorganic materials have been the core elements of nanotechnology because they exhibit unique photonic, electronic and stimuli-sensitive properties depending on their sizes, shapes and chemical characteristics. Beyond the synthesis and utilization of single colloids, the organization of colloidal nanoparticles while controlling their combination and spatial distribution in a system is attracting much interest to achieve unusual nano- and micro-structures and practical applications of the functionalities of colloidal nanoparticles.

The organization of colloidal nanoparticles includes the assembly of colloids

with the attachment of building units and the arrangement of nanoparticles into periodic arrays. By employing colloidal nanoparticles as nanoscale building blocks, organized colloidal superstructures can be assembled depending on the interaction between colloidal nanoparticles. The controlled assembly of colloidal nanoparticles enables the production of nature-mimic hierarchical structures and periodic structures with photonic properties. The arrangement of colloids on a solid substrate offer the control of the interparticle distance which is essential to utilize the functionalities of colloidal nanoparticles in device applications as the photonic and electronic properties of colloidal nanoparticles are modified by the interparticle coupling, which is affected by the distance between the colloids. Nanostructures of arranged colloidal nanoparticles on the nanoscale can also be applied as nanomasks and nanotemplates for the fabrication of the nanostructures of other materials.

Various colloidal nanoparticles, such as metal nanoparticles and polymeric colloids, serve as building blocks for the construction of organized colloidal structures. Given that block copolymers self-assemble into nanometer-sized micelles with soluble corona blocks and insoluble core blocks in a solvent which is selective for one of the blocks, block copolymer micelles can be utilized as a type of polymeric colloidal nanoparticles. In addition, block copolymer micelles can be applied as templates for the creation of organized metal and inorganic colloidal nanomaterials.

In this thesis, we focus on the development of organized structures of colloidal nanoparticles through the use of diblock copolymer micelles. Diblock copolymer

micelles, as colloidal building blocks, assemble into colloidal superstructures with controlled morphologies in a solution. We also demonstrate the utilization of diblock copolymer micelles as colloidal templates for the synthesis and arrangement of metal nanoparticles on solid substrates. Metal nanoparticle arrays created from a thin film of diblock copolymer micelles were further combined with fluorophore-encapsulating diblock copolymer micelles to control the interaction between the metal colloids and light emitters through micellar nanostructures, suggesting the potential application for the effective control of the fluorescence.

In chapter 1, we offer an overview of the self-associating characteristics of diblock copolymers, which assemble into micelles with soluble coronas and insoluble cores in a selective solvent for one of the blocks. The structure and dimension of block copolymer micelles can be precisely tuned by the molecular weight of polymers and the weight ratio of the blocks. These diblock copolymer micelles can be potentially employed as nano-sized polymeric colloids. Since diblock copolymer micelles can include functional substances, e.g. organic dyes and inorganic precursors, in their core blocks, they are beneficial as colloidal templates for arranging and organizing other colloidal nanomaterials in ordered arrays.

In chapter 2, we demonstrate supracolloidal polymer chains of diblock copolymer micelles. With a diblock copolymer composed of a polar block and a non-polar block, typical spherical micelles were initially obtained in a selective solvent for a non-polar block. We cross-linked the polar core of diblock copolymer

micelles and then made the solvent preferable to the core block but still compatible with the corona block. The cross-linked core was not dissolved by the favorable solvent but was exposed to the solvent when the corona was rearranged into two separate patches. In other words, typical spherical micelles were converted to colloidal micelles with the corona reorganized into two non-polar patches and the central core directly exposed to the solvent. With the reorganized micelles as colloidal monomers, we were able to polymerize their linear supracolloidal chains by increasing the polarity of the solvent. Furthermore, we applied the same protocol to diblock copolymers of a lower molecular weight and produced small colloidal monomers which were then combined with large colloidal monomers for the synthesis of supracolloidal random and block copolymers.

In chapter 3, we synthesize a diblock copolymer, consisting of one block which allows the synthesis of nanoparticles and another block which is selectively removable, by means of the reversible addition-fragmentation chain transfer (RAFT) polymerization. Using a selective solvent for each block, we produced two types of spherical micelles with an inverse position of two blocks, that is, the core of the nanoparticle-synthesizable block and the corona of the removable block and vice versa. We then coated single layers of these two micelles onto substrates, which were successfully employed as templates for the arrangement of spherical gold nanoparticles and their ring-like configuration over a large area.

In chapter 4, we utilize diblock copolymer micelles to organize metal nanoparticle arrays on a solid substrate which can be applied for the plasmon-

coupled fluorescence. A single layer of diblock copolymer micelles containing metal precursors in the core blocks was coated onto a solid substrate. The nanostructures of the micellar arrays of diblock copolymers were transferred to metal nanoparticle arrays by the reduction of metal precursors and the elimination of the polymers. The distance between the metal nanoparticles was controlled by the intermicellar distance in a single layer of diblock copolymer micelles. These metal nanoparticle arrays were applied as a seed substrate for the growth of larger metal nanoparticles with controlled size and interparticle distances. Diblock copolymer micelles were also used for the isolation of organic fluorophores in the micellar cores. A thin film of diblock copolymer micelles with organic dyes was combined with metal nanoparticle arrays to verify the strategy of metal-coupled fluorescence enhancement.

Keywords: Colloid nanoparticle, Colloidal assembly, Diblock Copolymer, Micelle, Self-assembly, Supracolloidal polymers, Metal nanoparticle, Fluorescence

Student Number: 2008-20313

Contents

List of Figures

Chapter 1

Chapter 2

Chapter 3

Chapter 4

Chapter 1

Introduction

1.1. Research Backgrounds

Colloidal nanoparticles, such as metal nanoparticles and polymeric colloids, have received a considerable amount of interest as constituent nanoscale materials in nanotechnology systems. A variety of colloidal nanoparticles based on organic and inorganic materials enable the creation of a library categorized by sizes, shapes and functionalities.[1-4] For example, colloids of gold nanoparticles are defined as spheres, nanorods, or polyhedral shapes with controlled dimensions.[5] Their unique photonic properties depending on their sizes and shapes are useful when applied to optoelectronic devices and sensors.[6-8]

In addition to the utilization of individual colloids, colloidal particles can serve as building blocks for organized structures ranging from clusters[9,10] to hierarchical architectures[11] with uniformity and complexity. The assembly of colloidal building blocks can demonstrate peculiar morphologies of colloidal superstructures in 1D, 2D or 3D,[12] providing the realization of hierarchical structures which mimic nature.[13] Because ensembles of colloidal nanoparticles have synergetic properties, e.g. a large enhancement of the electromagnetic field at hot spots[14] and Fano resonance,[15] colloidal superstructures have been successfully introduced in sensors, showing high performances.[16] Ordered arrays of colloids on solid substrates can also be directly used as not only functional substrates with photonic activity[17] but also as nanomasks for lithographic patterns[18] and as nanotemplates[19] for nanoscale structures of other materials.

Individual colloids or structures of arranged colloids can be fabricated by top-

down approaches such as photolithography and e-beam lithography though this processes are practically restricted to solid states on substrates.[20,21] A promising method for the effective establishment of colloidal systems is the bottom-up approach, which is feasible with both organic and inorganic nanoparticles. Recent advances in colloidal synthesis in a controlled manner have enabled the fabrication of colloidal nanoparticles with regular dimensions ranging from tens to hundreds of nanometers. Metal colloids have a variety of shapes and sizes depending on the chemical characteristics and the amount of surfactants and additives, as well as the use of synthetic processes with or without seeds.[3,5,22] Soft colloids are simply fabricated using molecular surfactants.[23] Polymers can be introduced to create soft colloids by means of emulsion polymerization or by the cross-linking of polymer chains.[24,25] Organized superstructures of these colloidal nanoparticles have been achieved by the alignment of colloidal building units along an external field or by directed self-assembly driven by the attractive interaction between the chemically modified surface of the colloids.[26,27]

Self-assemblies of block copolymers are potential candidates for use as nano-sized polymeric colloids. Block copolymers, which have two or more chemically different homopolymers which are covalently bonded, spontaneously self-assemble into periodic nanostructures with a regular size and morphology.[28,29] In a solvent that dissolves one of the blocks selectively, block copolymers self-associate into micelles with a soluble corona block and an insoluble core. The dimensions of block copolymer micelles are precisely tunable on the nanometer scale by

controlling the molecular weight. In addition, the shape of block copolymer micelles are controlled to form spheres or cylinders according to the volume ratio of the blocks.[30]

Block copolymer micelles can be employed as colloidal containers which can include various functional nanomaterials, e.g. organic dyes and inorganic precursors which are insoluble in solvents, in their core blocks such that they are beneficial as functional colloids when applied in further applications.[28,29,31,32] These functionalized block copolymer micelles can be transferred onto solid substrates by simple coating methods, such as Langmuir-Blodgett (LB), dip-coating, or spin-coating to form a variety of nanostructures.[28,33,34] Micellar nanostructures on solid substrates can be used as nanoscale lithographic mask in etching processes and as templates for the in-situ synthesis of nanoparticles of metal, semiconductors, or oxides into micellar cores with or without removal of the copolymer template.[35-37]. Thus, block copolymer micelles can act as colloidal templates which can be used to arrange and organizeordered colloidal structures of other colloidal nanomaterials.

In this thesis, we focus on the development of organized structures of colloidal building blocks through the utilization of diblock copolymer micelles in a solution and on a solid substrate. Diblock copolymer micelles, as a colloidal building block, assemble into colloidal superstructures with controlled morphologies in a solution. We also demonstrate the use of diblock copolymer micelles as templates for the synthesis and arrangement of inorganic colloids on solid substrates. Metal colloids

arranged by diblock copolymer micelles are further combined with fluorophores-encapsulating diblock copolymer micelles for the control of the interaction between metal colloids and light emitters by micellar nanostructures, suggesting an application for the effective control of fluorescence.

1.2. Self-assembled Micelles of Diblock Copolymers

As noted in the previous section, a diblock copolymer is composed of two chemically different polymers linked by a covalent bond. The microphase separation of diblock copolymers is managed by the enthalpy arising when mixing constituent blocks and the entropic penalty related to the chain length. These thermodynamic terms of enthalpy and entropy are proportional to the Flory-Huggings interaction parameter (χ) and the degree of polymerization (N) respectively such that the phase behavior of block copolymers can be predicted by the product χN, which denotes the enthalpy-entropy balance.[29,38]

With the segregation of dissimilar polymer blocks in a diblock copolymer, block copolymers are self-associated into structures with internal domains with nanoscale lengths. Self-assembled diblock copolymers form various nanostructures such as lamellae (LAM), modulated lamellae (MLAM), perforated layers (PLAM), hexagonally ordered cylinders (HEX), arrays of spherical microdomains (BCC) and bicontinuous gyroids in a bulk and spherical and cylindrical micelles (MIC)

and vesicles in a solution.[39-41]

Block copolymers in a diluted solution self-associate into micelles with coronas of the soluble block and cores of the insoluble block in a selective solvent that dissolves only one block above a concentration termed the criticial micelle concentration (cmc).[42] The size and structure of micelles are determined by the molecular weight of each block, the volume ratio between the blocks, the chemical affinity of each block to the solvent and the chemical miscibility between the blocks.[43]

A diblock copolymer is presented as A-B. In a selective solvent for B blocks, the micelle consists of an A-rich core and a B-rich corona. Depending on the domain sizes of the cores and coronas, two boundary models, hairy micelles and crew-cut micelles, have been introduced. A hairy micelle has a much larger corona than its core, whereas a crew-cut micelle has a larger core than its corona.[44,45]

Regardless of whether the micellar structure is the hairy or crew-cut type, amphiphilic block copolymers form “amphiphilic micelles” composed of a core with only an A block and a corona with only a B block. The micellization of amphiphilic block copolymers is driven by the strong segregation of A and B blocks, which is characterized by a large interaction parameter χN ($\gg$ 10) due to the energy penalty of the A-solvent interaction and the compatibility of the B-solvent with high interfacial energy between the A-B blocks.[45]

We can introduce an aggregation number, Z, which is the number of block copolymer molecules in a micelle, to characterize the structure of diblock

copolymer micelles. The aggregation number (Z) of amphiphilic micelles is proportional to the square of the degree of polymerization (N^2), corresponding to a strong segregation limit regime.[38,45] Specifically, the aggregation number for amphiphilic molecules can be quantitatively expressed by the degree of polymerization of each block as in an earlier work.[45]

$$Z = Z_0 N_A^{\alpha} N_B^{\beta} \qquad (1\text{-}1)$$

In this equation, Z_0 is related to the interaction parameter χ and the local packing parameter as expressed in the aforementioned study.[45]

$$Z_0 = 36\pi\Delta_0^3, \quad \Delta_0^3 = \frac{\nu_0^{2/3}}{b_0^3} \quad (1\text{-}2)$$

Here, Δ_0 is a dimensionless intrinsic patching parameter of a specific block copolymer and solvent system. It is notable that equation 1-1 and 1-2 are universal in the system of strong segregating amphiphilic molecules including diblock, triblock and graft copolymers as well as low molecular surfactants. The aggregation number of various amphiphilic structures versus the degree of polymerization of the A block is fitted onto a single plot of the equation.[45] For many micellar systems, the exponents α and β are close to 2.0 and 0.8, respectively.[45]

The aggregation number as calculated by equation 1-1 and 1-2 enable the calculation of the core radius (R_c) via the space filling condition for the core and the corona dimension (D_h) for the swollen block in good solvents, approximately,[45]

$$\frac{4\pi}{3} R_c^3 = ZN_A v_0 \quad (1\text{-}3)$$

$$D_h \approx Z^{0.2} N_B^{0.6} \quad (1\text{-}4)$$

where v_0 is the molar volume of core monomers.

The relationship between the core and corona dimension of the micellar nanostructures and the degree of polymerization of the block copolymers implies the manipulation of the sizes of the micelles by the molecular weight of block copolymers. The value of Z_0 of a variety of block copolymers is tabulated such that the preparation of diblock copolymer micelles with desired dimensions of the core and the corona, as colloidal substances, is promising for further potential applications in colloidal systems.

1.3. Colloidal Nanomaterials with Diblock Copolymer Micelles

Colloids of diblock copolymer micelles

Self-assembled micelles of diblock copolymers can be directly used as polymeric colloidal nanoparticles because the dimensions of diblock copolymer micelles are on the nanometer scale, allowing them to be categorized as colloids. Micellar nanostructures of diblock copolymers are practically controlled by the molecular weight of copolymer chains, by the volume ratio between each block and by chemical environment.[30,40,45] For example, polystyrene-poly(4-

vinylpyridine), PS-P4VP, self-assembles into spherical micelles in toluene which is a selective solvent for the PS block. The sizes of the core and the corona of PS-P4VP micelles are determined by the molecular weights of the PS block and the P4VP block (Figure 1.1). Because the nanostructures of micelles are also affected by the solvent, the sizes of the micelles depend on the preparation condition of micelles such as the solvent exchange.[46] For PS-P4VP, micellization by solvent exchange from chloroform, a co-solvent of both PS and P4VP, to toluene results in smaller PS-P4VP micelles compared to the direct dissolution of PS-P4VP into PS-selective toluene (Figure 1.2). The solvent is also important when controlling the shapes of micelles; for example, the existence of a solvent to dissolve P4VP determines the creation of spherical or cylindrical PS-P4VP micelles with the same molecular weight.[47] Nanostructures of block copolymer micelles which have stimuli-responsive blocks can also be manipulated by a change in external conditions such as the pH or the temperature such that they are potentially applied in the further applications for drug delivery and biosensors.[48,49]

Block copolymer micelles can be employed as colloidal building blocks for colloidal assemblies. Triblock copolymers are useful for the synthesis of micelles with extraordinary structures, such as disks and Janus micelles.[50,51] These micelles have compartmentalized surface with different physical or chemical characteristics such that anisotropic superstructures of micellar colloids can be formed by means of site-selective interactions between micelles.[50,52,53] Diblock copolymer micelles can also assemble into controlled superstructures such as one-

dimensional chains and wires driven by guided assembly with molecular templates, crystallization or π-π interaction.[54-56] A two-dimensional organization of diblock copolymer micelles on a solid substrate can also be guaranteed by a simple coating methods.[28,33-37] These micellar colloids arranged on a substrate are useful for nanomasks or nanotemplates with which to fabricate nanostructures of inorganic colloidal materials.[28,33-37]

Inorganic colloids in diblock copolymer micelles

With respect to potential applications of diblock copolymer micelles, inorganic precursors can be incorporated into block copolymer micelles.[28,33-37,57] Holding inorganic substances in diblock copolymer micelles is achievable by introducing functional blocks which have chemical or physical compatibility with inorganic moieties, such as dipolar interaction, hydrogen bonding, coordination or covalent bonding.[29] By stirring the precursor salts in a micellar solution, the precursor can be incorporated into the micelles. Inorganic precursors can be included in the core, corona or interfacial area of core and corona selectively by controlling the location of compatible blocks in the micellar nanostructure.[58]

Incorporated inorganic precursors can be turned into inorganic colloidal nanoparticles by means of reduction processes. Chemical reducing agents, e.g. $NaBH_4$ and hydrazine, are useful to synthesize inorganic nanoparticles in diblock copolymer micelles.[28,33-37] Diblock copolymer micelles with inorganic

precursors can be transferred to a solid substrate by a simple coating method such that precursors isolated in micelles can be reduced by a plasma treatment and/or heat treatment to create inorganic colloidal arrays without polymeric micelles on a solid substrate.[28,33-37] For example, $SiCl_4$, a precursor of SiO_2 nanoparticles, can be selectively included in the core block of PS-P4VP micelles. PS-P4VP micelles containing $SiCl_4$ can be coated on Si wafers or quartz by spin coating to fabricate a single layer of micelles in a thin film. After O_2 plasma treatment, all the polymers are removed and pseudo-hexagonal arrays of SiO_2 nanoparticles are generated (Figure 1.3). The sizes of SiO_2 nanoparticles and interparticle distances can be manipulated by the molecular weight of PS-P4VP as shown in Figure 1.3. (It is noted that PS(51)-P4VP(18) micelles and PS(109)-P4VP(27) micelles in Figure 1.3 were fabricated in terms of the direct dissolution of polymer powders in toluene.)

Fluorescent micellar colloids of diblock copolymers

The amphiphilicity of diblock copolymer micelles can solubilize organic molecules which are insoluble in a solvent.[32,32] A typical case is one in which fluorescent dyes are insoluble in a nonpolar solvent such as toluene, whereas the same dyes can be encapsulated into the P4VP core block of PS-P4VP micelles, becoming well dispersed in a nonpolar solvent with bright fluorescence (Figure 1.4). Thus, the encapsulation of fluorescent dyes into diblock copolymer micelles can be applied for the post-functionalization of optically inert block copolymer

micellar colloids. Because a small amount of an organic additive in the core of micelles does not affect anything on the micellar structures, it is possible to utilize fluorescent micellar colloids with different emission wavelength in the same micellar nanostructure. The same fluorescent property with different micellar nanostructures is also conceivable. The utilization of diblock copolymer micelles encapsulating fluorophores provides fluorescent nanostructures with fixed nanoscale dimension which is advantageous when studying the FRET and surface-plasmon-coupled fluorescence of functional nanomaterials, such as fluorescent dyes, QDs and metal nanoparticles, as the photonic coupling strongly depends on the distance between the functional nanomaterials.[59-61]

1.4. References

[1] J. Goesmann, C. Feldmann, *Angew. Chem. Int. Ed.* **2010**, *49*, 1362.

[2] J. N. Anker, W. P. Hall, O. Lyandres, N. C. Shah, J .Zhao, R. P. van Duyne, *Nat. Mater.* **2008**, *7*, 442.

[3] M. Rycenga, C. M. Cobley, J. Zeng, W. Li, C. H. Moran, Q. Zhang, D. Qin, Y. Xia, *Chem. Rev.* **2011**, *111*, 3669

[4] N. Vogel, C. K. Wiess, K. Landfester, *Soft Matter* **2012**, *8*, 4044.

[5] M. Grzelczak, J. Pérez-Juste, P. Mulvaney, L. M. Liz-Marzán, *Chem. Soc. Rev.* **2008**, *37*, 1783.

[6] E. Hutter, J. H. Fender, *Adv. Mater.* **2004**, *16*, 1685.

[7] E. Ozbay, *Science* **2006**, *331*, 189.

[8] S. Lal, S. Link, N. J. Halas, *Nat. Photonics* **2007**, *1*, 641.

[9] M. Grzelczak, J. Vermant, E. M. Furst, L. M. Liz-Marán, *ACS Nano* **2010**, *4*, 3591.

[10] S. Sacanna, D. J. Pine, G. R. Yi, *Soft Matter* **2013**, *9*, 8096.

[11] R. C. Hayward, D. J. Pochan, *Macromolecules* **2010**, *43*, 3577.

[12] Z. Nie, A. Petukhova, E. Kumacheva, *Nat. Nanotechonol.* **2010**, *5*, 15.

[13] S. Mann, *Chem. Commun*. **2004**, 1.

[14] J. H. Yoon, J. Lim, S. Yoon, *ACS Nano* **2012**, *6*, 7199.

[15] M. Hentschel, M. Saliba, R. Vogelgesang, H. Giessen, A. P. Alivisatos, N. Liu, *Nano Lett.* **2010**, *10*, 2721.

[16] A. F. Stewart, A. Lee, A. Ahmed, S. Ip, E. Kumacheva, G. C. Walker, *ACS*

Nano **2014**, *8*, 5462.

[17] C. I. Aguirre, E. Reguera, A. Stein, *Adv. Funct. Mater.* **2010**, *20*, 2565.

[18] J. P. Wang, K. Y. Lai, Y. R. Lin, C. A. Lin, J. H. He, *Langmuir* **2010**, *26*, 12855.

[19] B. Ding, C. Hrelescu, N. Arnold, G. Isic, T. A. Klar, *Nano Lett.* **2013**, *13*, 378.

[20] Q. Zhu, S. Zheng, S. Lin, T. R. Liu, C. Jin, *Nanoscale* **2014**, *6*, 7237.

[21] Q. H. Wei, K. H. Su, S. Durant, X. Zhang, *Nano Lett.* **2004**, *4*, 1067

[22] M. N. O'Brien, M. R. Jones, K. A. Brown, C. A. Mirkin, *J. Am. Chem. Soc.* **2014**, *136*, 7603.

[23] M. P. Pileni, *Nat. Mater.* **2003**, *2*, 145.

[24] J. P. Rao, K. E. Geckeler, *Prog. Polym. Sci*. **2011**, *36*, 887.

[25] R. K. O'Reilly, C. J. Hawker, K. L. Wooley, *Chem. Soc. Rev.* **2006**, *35*, 1068.

[26] Y. Min, M. Akbulut, K. Kristiansen, Y. Golan. J. Israelachvili, *Nat. Mater.* **2008**, *7*, 527.

[27] S. C. Glotzer, M. J. Solomon, *Nat. Mater*. **2007**, *6*, 557.

[28] R. Glass, M. Möller, J. P. Spatz, *Nanotechnology* **2003**, *14*, 1153.

[29] S. Föster, T. Plantenberg, *Angew. Chem. Int. Ed.* **2002**, *41*, 689.

[30] A. Blanazs, S. P. Arms, A. J. Ryan, *Macromol. Rapid Commun.* **2009**, *30*, 267.

[31] S. I. Yoo, S. H. Bae, K. S. Kim, B. H. Sohn, *Soft Matter* **2009**, *5*, 2990.

[32] C. Li, J. Hu, S. Liu, *Soft Matter* **2012**, *8*, 7096.

[33] S. Jain, F. S. Bates, *Macromolecules* **2004**, *37*, 1511.

[34] A. Böker, A. H. E. Müller, G. Krausch, *Macromolecules* **2001**, *34*, 7477.

[35] X. Li, K. H. A. Lau, D. H. Kim, W. Knoll, *Langmuir* **2005**, *21*, 5212.

[36] W. J. Cho, Y. Kim, J. K. Kim, *ACS Nano* **2012**, *6*, 249.

[37] S. H. Yun, S. I. Yoo, J. C. Jung, W. C. Zin, B. H. Sohn, *Chem. Mater.* **2006**, *18*, 5646.

[38] F. S. Bates, G. H. Fredrickson, *Annu. Rev. Phys. Chem.* **1990**, *41*, 525.

[39] S. B. Darling, *Prog. Polym. Sci.* **2007**, *32*, 1152.

[40] Y. Mai, A. Eisenberg, *Chem. Soc. Rev.* **2012**, *41*, 5969.

[41] S. Förster, M. Konrad, *J. Mater. Chem.* **2003**, *13*, 2671.

[42] G. Riess, *Prog. Polym. Sci.* **2003**, *28*, 1107.

[43] E. B. Zhulina, M. Adam, I, LaRue, S. S. Sheiko, M. Rubinstein, *Macromolecules* **2005**, *38*, 5330.

[44] M. Antonietti, S. Heinz, M. Schmidt, C. Rosenauer, *Macromolecules* **1994**, *27*, 3276.

[45] S. Förster, M. Zisenis, E. Wenz, M. Antonietti, *J. Chem. Phys.* **1996**, *104*, 9956.

[46] E. G. Kelley, R. P. Murphy, J. E. Seppala, T. P. Smart, S. D. Hann, M. O. Sullivan, T. H. Epps, *Nat. Commun.* **2014**, *5*, 3599.

[47] N. Ali, S. Y. Park, *Langmuir* **2008**, *24*, 9279.

[48] Z. Ge, S. Liu, *Chem. Soc. Rev.* **2013**, *42*, 7289.

[49] M. A. C. Stuart, W. T. S. Huck, J. Genzer, M. Müller, C. Ober, M. Stamm, G. B. Sukhorukove, I. Szleifer, V. V. Tsukruk, M. Urba, F. Winnik, S. Zauscher, I. Luzinov, S. Minko, *Nat. Mater.* **2010**, *9*, 101.

[50] H. Cui, Z. Chen, S. Zhong, K. L. Wooley, D. J. Pochan, *Science* **2007**, *317*, 647.

[51] A. Walther, M. Drechster, S. Rosenfeldt, L. Harnau, M. Ballauff, V. Abetz, A. H. E. Müller, *J. Am. Chem. Soc.* **2009**, *131*, 4720

[52] A. H. Gröschel, F. H. Schacher, H. Schmalz, O. V. Borisov, E. B. Zhulina, A. Walther, A. H. E. Müller, *Nat. Commun.* **2012**, *3*, 710.

[53] A. H. Gröschel, A. Walther, T. I. Löbling, F. H. Schacher, H. Schmalz, A. H. E. Müller, *Nature* **2012**, *503*, 247.

[54] K. Zhang, H. Miao, D. Chen, *J. Am. Chem. Soc.* **2014**, *136*, 15933.

[55] J. Qian, Y. Lu, A. Chia, M. Zhang, P. A. Rupar, N. Gunari, G. C. Walker, G. Cambridge, F. He, G. Guerin, I. Manners, M. A. Winnik, *ACS Nano* **2013**, *7*, 3754.

[56] K. Y. Yoon, I. H. Lee, K. O. Kim, J. Jang, E. Lee, T. L. Choi, *J. Am. Chem. Soc.* **2012**, *134*, 14291.

[57] G. Rainò, T. Stöferle, C. Park, H. C. Kim, T. Topuria, P. M. Rice, I. J. Chin, R. D. Miller, R. F. Mahrt, *ACS Nano* **2011**, *5*, 3536.

[58] Y. Liu, X. Wang, *Polym. Chem.* **2011**, *2*, 2741

[59] S. I. Yoo, S. J. An, G. H. Choi, K. S. Kim, G. C. Yi, W. C. Zin, J. C. Jung, B. H. Sohn, *Adv. Mater.* **2007**, *19*, 1594.

[60] K. S. Kim, J. H. Kim, H. Kim, F. Laquai, E. Arfin, J. K. Lee, S. I. Yoo, B. H. Sohn, *ACS Nano* **2012**, *6*, 5051.

[61] K. S. Kim, H. Kim, J. H. Kim, J. H. Kim, C. L. Lee, F. Laquai, S. I. Yoo, B. H. Sohn, *J. Mater. Chem.* **2012**, *22*, 24727.

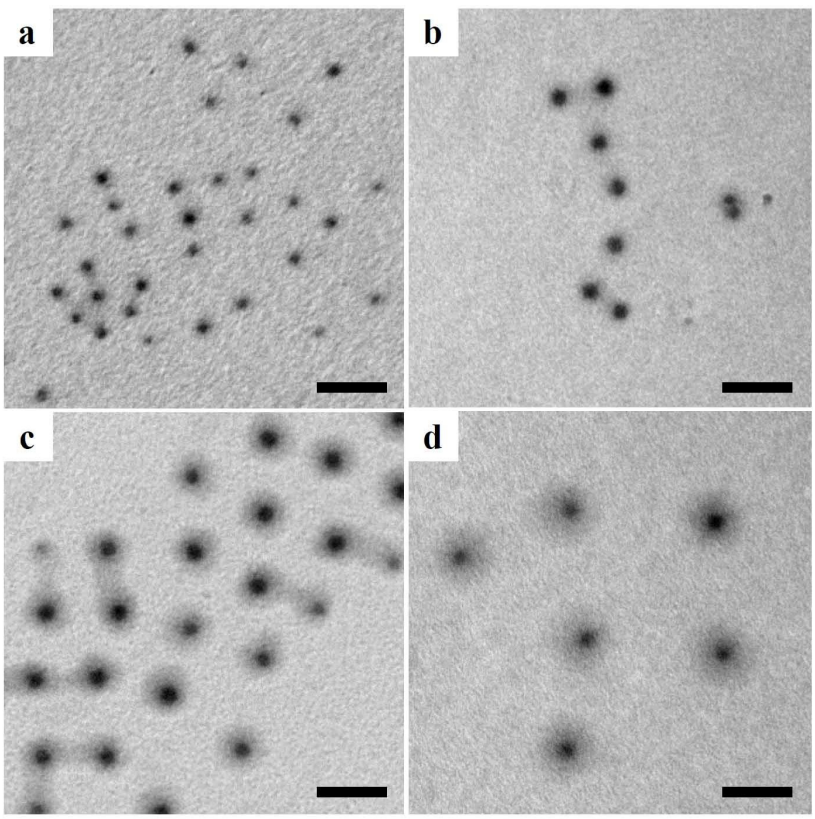

Figure 1.1. TEM images of PS-P4VP micelles; (a) PS(25)-P4VP(7); (b) PS(41)-P4VP(24); (c) PS(109)-P4VP(27); (d) PS(252)-P4VP(43). The number in the parenthesis is a number average molecular weight in kg/mol. P4VP core blocks were selectively stained by I_2 vapor. All scale bars are 100 nm.

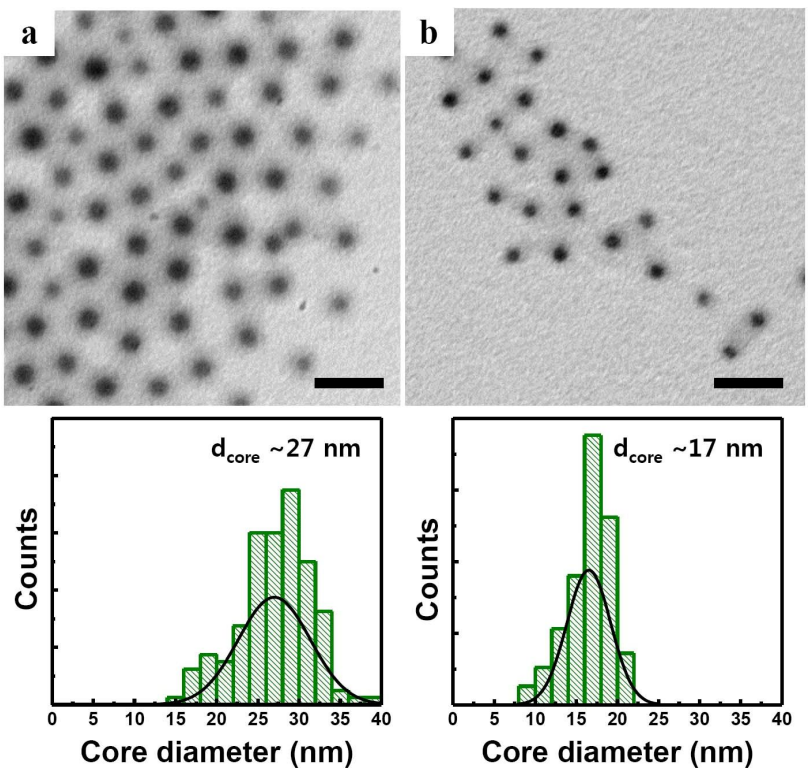

Figure 1.2. TEM images (top) and the distribution of the core diameter of PS(51)-P4VP(18) micelles; micelles were formed by (a) direct dissolution in toluene and (b) solvent exchange from chloroform to toluene. P4VP core blocks were selectively stained by I_2 vapor. All scale bars are 100 nm.

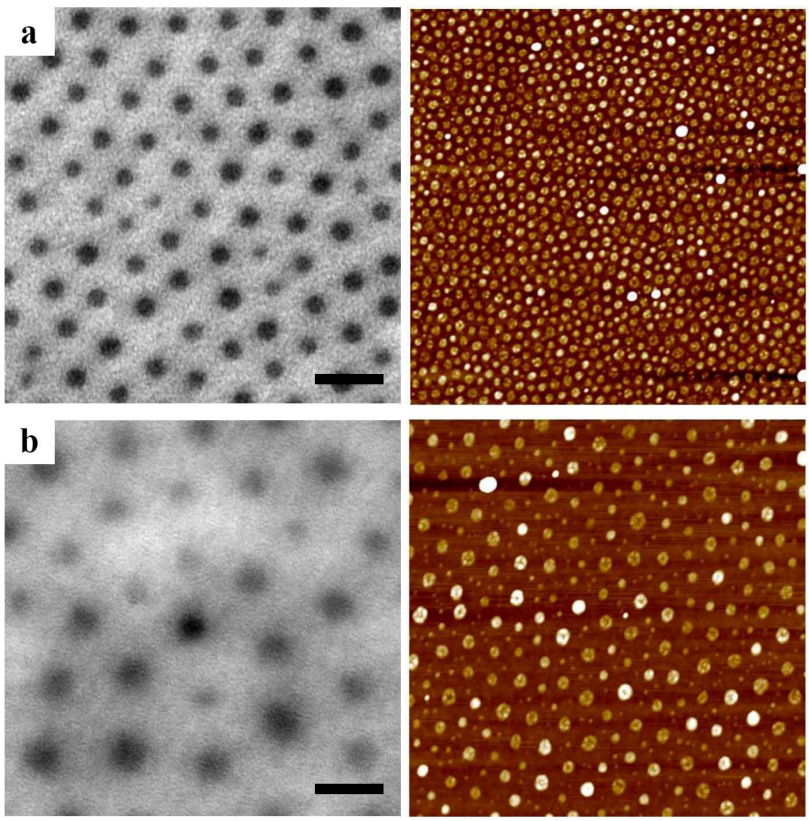

Figure 1.3. TEM images of a thin film of neat PS-P4VP micelles (left) and AFM images of SiO_2 nanoparticle arrays (right) fabricated from a thin film of $SiCl_4$-including PS-P4VP micelles. (a) PS(51)-P4VP(18); (b) PS(109)-P4VP(27). P4VP core blocks were selectively stained by I_2 vapor. All scale bars are 100 nm. The size of each AFM image is 2 μm by 2 μm.

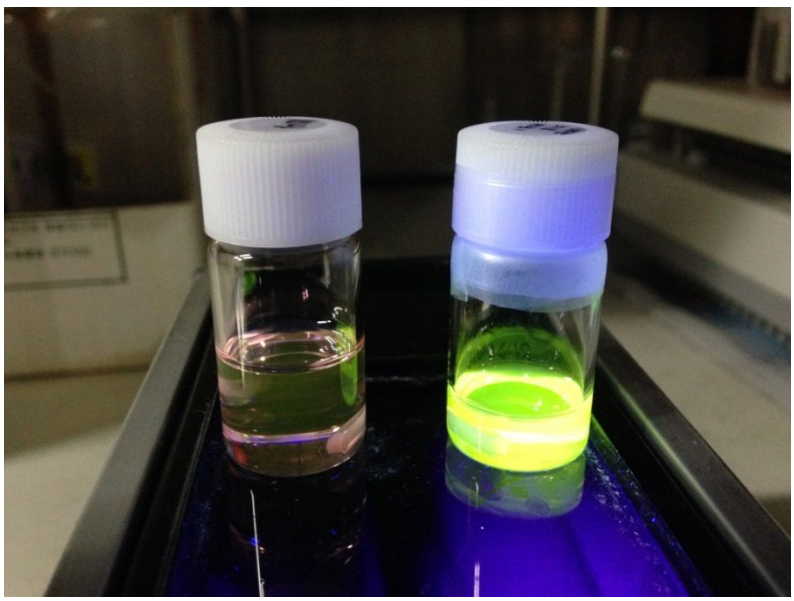

Figure 1.4. The picture of toluene solution with rhodamine 123 (left) and PS(51)-P4VP(18) micelles encapsulating rhodamine 123 (right) on a hand UV lamp (365 nm).

Chapter 2

Supracolloidal Polymer Chains of Diblock Copolymer Micelles

2.1. Introduction

Colloidal nanoparticles such as spherical gold nanoparticles and one-dimensional gold nanorods self-assemble into various superstructures from aggregated clusters to organized superlattices.[1-3] Self-organized superstructures of colloidal nanoparticles depend on attraction and repulsion between colloidal building blocks.[4-6] For example, non-directional attraction induces aggregated clusters of nanoparticles whereas strong repulsive interaction makes colloidal nanoparticles stable in solution without forming a superstructure. In particular, directional attraction between nanoparticles with orthogonal repulsion to the attraction can produce a chain-like supracolloidal polymer. A representative example in this situation is a supracolloidal polymer chain of gold nanorods, which were mainly stabilized by polar surfactants, with their two ends selectively covered by non-polar polymers.[7,8] By increasing the polarity of the solvent around the gold nanorods, attraction between the non-polar polymers at the ends of neighboring nanorods was generated due to unfavorable contacts of the polymer with the solvent. However, the lateral sides of gold nanorods were stabilized by polar surfactants so that gold nanorods were connected linearly to form a supracolloidal polymer chain. The strategy of balancing attraction and repulsion to guide a linear superstructure was recently applied to spherical gold nanoparticles to produce their supracolloidal polymer chains.[9,10]

With polymeric colloidal nanoparticles including polymerization-induced self-assemblies,[11-14] various superstructures such as chains, ribbons, and worms

have been reported.[11-20] Especially, by controlling attraction and repulsion of spherical micelles of triblock copolymers, hierarchically co-assembled suprachains as well as supracolloidal polymer chains were demonstrated.[21,22] In a non-solvent for the central block, triblock copolymers formed spherical micelles that consisted of the insoluble core and the compartmentalized corona with polar patches and non-polar patches. By increasing the polarity of the solvent, the non-polar compartments in the corona generated attraction between the micelles but the polar compartments produced repulsion to avoid non-directional aggregation so that the micelles organized into a linear supracolloidal chain. The approach with triblock copolymers enabled the precise controllability on the nanoscale compartments in the corona of the micelles, although the synthesis of triblock copolymers would not be trivial.

In this chapter, we demonstrate supracolloidal polymer chains of diblock copolymer micelles. With a diblock copolymer composed of a polar block and a non-polar block, typical spherical micelles were first obtained in a selective solvent for the non-polar block. Since diblock copolymer micelles have a simple nanostructure of the core and the corona, prediction of the size of micelles depending on the molecular weights is rather straightforward and there are many choices for a micelle-forming solvent. With diblock copolymer micelles, we cross-linked the polar core and then made the solvent preferable to the core block but still compatible with the corona block. The cross-linked core was not dissolved by the favorable solvent but it was exposed to the solvent by rearranging the corona into

two separated patches. In other words, usual spherical micelles were converted to colloidal micelles with the corona reorganized into two non-polar patches and the central core that was directly exposed to the solvent. With the reorganized micelles as colloidal monomers, we were able to polymerize their linear supracolloidal chains by increasing the polarity of the solvent. Furthermore, we applied the same protocol to diblock copolymers having a lower molecular weight and produced small colloidal monomers which were then combined with large colloidal monomers for the synthesis of supracolloidal random and block copolymers.

2.2. Experimental Section

Cross-linked PS-P4VP micelles

Diblock copolymers of polystyrene-poly(4-vinylpyridine), PS(51)-P4VP(18) and PS(25)-P4VP(7), were purchased from Polymer Source, Inc. The number in the parenthesis is a number average molecular weight in kg/mol. The polydispersity index (PDI) is 1.15 for PS(51)-P4VP(18) and 1.10 for PS(25)-P4VP(7). We first dissolved PS-P4VP copolymers in chloroform, which is a co-solvent for both PS and P4VP blocks, to yield a 0.2 wt% solution. Then, we added toluene, which is a selective solvent for the PS block, to the solution with stirring until the weight ratio of toluene to chloroform reached to 0.2. After mixing, chloroform was completely evaporated at 80 ℃ to obtain a 1.0 wt% toluene solution of PS-P4VP micelles. For cross-linking the P4VP core, 1,4-dibromobutane (DBB) was added to the micellar solution with a molar ratio of DBB to 4VP equal to 0.5 which can fully quarternize the 4VP units in the copolymer, followed by stirring at 45 ℃ for 48 hr. The same procedure was applied to both PS(51)-P4VP(18) and PS(25)-P4VP(7).

Colloidal monomers of PS-P4VP micelles

To produce colloidal monomers, we changed the polarity of the solvent by adding DMF to a 1.0 wt% toluene solution of cross-linked PS-P4VP micelles with 100 times of DMF to toluene in weight, resulting in a 0.01 wt% solution of colloidal monomers of PS-P4VP micelles with the reorganized corona of two PS

patches. The same condition was used for PS(51)-P4VP(18) and PS(25)-P4VP(7).

Supracolloidal polymers of colloidal monomers of PS-P4VP micelles

We further increased the polarity of the solvent to synthesize supracolloidal polymer chains from colloidal monomers of PS(51)-P4VP(18) micelles by dropping a mixture of DI water and DMF (20 wt% water) to yield 10 wt% water in the final solution. The solution was kept without stirring at room temperature for 48 hr. For PS(25)-P4VP(7), a mixture of water and DMF containing 30 wt% water was dropped to yield 15 wt% water in the final solution.

Supracolloidal random and block copolymers

For supracolloidal random copolymerization, two colloidal monomer solutions of PS(51)-P4VP(18) and PS(25)-P4VP(7) were mixed in the same weight. Then, a mixture of water and DMF (30 wt% water) was dropped into the solution to obtain 15 wt% of water in the final solution. The solution was kept without stirring at room temperature for 24 hr. To synthesize supracolloidal block copolymers, we first prepared two homopolymer chains of colloidal monomers of PS(51)-P4VP(18) and PS(25)-P4VP(7) for 24 hr polymerization as described above. But both solutions had 15 wt% of water. Then, we mixed two solutions of supracolloidal homopolymers of PS(51)-P4VP(18) and PS(25)-P4VP(7) in the same weight. The mixed solution was kept without stirring at room temperature for additional 24 hr.

Characterization

Transmission electron microscopy (TEM) was performed on a Hitachi H-7600 at 100 kV. A TEM sample was prepared by dropping a solution of micelles or supracolloidal chains on a carbon-coated TEM grid with removal of excess solvent by a filter paper. After drying in air, the TEM sample was exposed to I_2 vapor for staining the P4VP block. Fourier transform infrared (FT-IR) spectra were obtained using a Nicolet iS10 FT-IR Spectrometer (Thermo Scientific). Dynamic light scattering (DLS) was carried out with a Zetasizer Nano-S Instrument (Malvern Instruments) at the fixed scattering angle of 173°.

2.3. Results and Discussion

We selected a diblock copolymer of polystyrene-poly(4-vinylpyridine) (PS-P4VP) which consists of a non-polar PS block and a polar P4VP block that can be effectively cross-linked with 1,4-dibromobutane (DBB).[23,24] First, a PS(51)-P4VP(18) micelle with the PS corona and the P4VP core was obtained in toluene which is a selective solvent for the PS block.[25] The number in the parenthesis is a number average molecular weight in kg/mol. The P4VP core was fully cross-linked with a molar ratio of DBB to 4VP equal to 0.5. Quaternization of the 4VP units was confirmed by decrease of the 4VP band at 1600 cm^{-1} and increase of the quaternized 4VP band at 1643 cm^{-1} (Figure 2.1).[26] The P4VP core was also stained with I_2 for TEM. In Figure 2.2a, a spherical micelle of the dark P4VP core with the grey PS corona is visible. Since the core is clearly discernible in the image, we obtained the average core diameter of 16.5 nm (± 2.7 nm) over a larger area than this image.

The solubility parameter of DMF (24.8 $MPa^{1/2}$) is close to that of P4VP (22.2 $MPa^{1/2}$) but somewhat larger than that of PS (18.6 $MPa^{1/2}$),[27,28] indicating that DMF is a good solvent for P4VP but a poor solvent for PS. That is, after the addition of DMF, the solvent around PS-P4VP micelles became preferable to the P4VP core. After changing the polarity of the solvent, as shown in the TEM image of Figure 2.2b, a spherical micelle was changed to a micelle with two separated patches of the PS block and the central P4VP core exposed to the solvent. With this micellar structure, the P4VP core can directly contact with the solvent. The

diameter of the P4VP core was basically unchanged.

Since the P4VP core was cross-linked, it was not dissolved by a favorable solvent of DMF. However, the P4VP core was exposed to DMF by rearranging the PS corona into two separated patches, i.e., by a pop-up structure of the P4VP core over the divided PS corona. Segregation of the PS corona initiated by the P4VP core can depend on the portion of the corona block to the total copolymer[22] which was 0.74 in terms of the molecular weight for PS(51)-P4VP(18). We observed that the core would not be able to divide the corona in a higher portion of the corona (0.85 for PS(109)-P4VP(27)) as shown in Figure 2.5a. With a lower portion of the corona (0.63 for PS(41)-P4VP(24)), more than two patches in the corona would be induced by the core (Figure 2.5b). We are currently investigating the patch formation in the corona depending on the portion of the corona block.

In the rearranged micellar structure shown in Figure 2.2b, two non-polar PS patches emanated from the core can act as attractive parts whereas the polar P4VP core, directly exposed to the solvent between two patches, can work as a repulsive part when the solvent becomes more polar by addition of water. We can consider this rearranged micellar structure an analogue of a polar-surfactant-stabilized Au nanorod with non-polar polymers attached to two ends[7] or a spherical triblock copolymer micelle having a divided corona with polar and non-polar compartments.[22] That is, the micelle with the non-polar patched corona and the polar core directly exposed to the solvent can be a colloidal monomer.

To increase the polarity of the solvent, we added water, which was diluted

with DMF, to these colloidal monomers of the rearranged micelles of PS(51)-P4VP(18). As shown in Figure 2.2c, a supracolloidal polymer chain was successfully synthesized. The image clearly shows alternating colloidal monomer units of PS(51)-P4VP(18) micelles. The inset in Figure 2.2c shows a representative chain of a whole polymer, which is ~8.9 μm long. The boxed area in the inset is the image shown in Figure 2.2c. A fully enlarged image of the inset is also given in Figure 2.3. By dynamic light scattering (DLS) measurements (Figure 2.4), we also observed the increase of the average diameter as the reaction proceeded, although DLS gives a spherical-averaged diameter that is equal to neither the chain length nor the chain width.[29] It is noted that we did not observe individual colloidal monomers which were not incorporated into supracolloidal chains. Several defects of joining more than two colloidal monomers can be found in the whole chain.

By addition of water, the non-polar patches of the PS block in the colloidal monomer became unfavorable to the contact with water so that attraction between the PS patches of neighboring colloidal monomers was exerted, leading to the reaction between the colloidal monomers. Simultaneously, the exposed P4VP core became more favorable to the contact with the solvent containing water so that lateral aggregation of the colloidal monomers was effectively prevented by the P4VP core exposed to the solvent. Thus, we effectively polymerized the colloidal monomers of the reorganized PS-P4VP micelles to a supracolloidal polymer chain.

We note that PS(51)-P4VP(18) micelles cross-liked by DBB of which the molar ratios to VP were 0.2 and 1.0 respectively were rearranged to micellar

colloids with the two nonpolar PS patches and polar central P4VP cores (Figure 2.6). These colloidal structures were the same to those of micellar colloids in Figure 2.2b so that both of micellar colloids were polymerized to form supracolloidal polymer chains by adding water, as shown in Figure 2.6, suggesting the rearranged micellar structure was not much affected with different amounts of cross-linking agents (the molar ratio of DBB to 4VP = 0.2~1.0).

We applied the same protocol to PS-P4VP having a lower molecular weight in order to obtain smaller colloidal monomers and their supracolloidal polymer chains. We selected PS(25)-P4VP(7) that has less than a half molecular weight of PS(51)-P4VP(18). However, the portion of the corona block to the total copolymer was similarly 0.78. Figure 2.7a shows smaller spherical micelles of the dark P4VP core (9.4 nm ± 1.7 nm in diameter) with the grey PS corona. We note that Figure 2.2 and Figure 2.7 are in the same scale for good comparison. After the polarity of the solvent was changed with DMF, smaller patched micelles compared to those of PS(51)-P4VP(18) were obtained as shown in Figure 2.7b. Thus, we produced smaller colloidal monomers consisting of two non-polar PS patches in the corona and the central P4VP core directly exposed to the solvent.

To polymerize these colloidal monomers of PS(25)-P4VP(7), we further changed the polarity of the solvent by adding water as before. But more water was necessary for the polymerization of these smaller monomers. As shown in Figure 2.7c, a supracolloidal polymer chain with smaller colloidal monomers was again synthesized, which has alternating colloidal units of PS(25)-P4VP(7) micelles.

Several polymer chains can be found in the inset of Figure 2.7c, which are clearly discernible in a fully enlarged image of Figure 2.8. The length of a whole polymer chain was ~2.8 μm, which was shorter than that of PS(51)-P4VP(18).

To obtain supracolloidal polymer chains of colloidal monomers of PS-P4VP after 48 hr polymerization (Figures 2c and 7c), 15 wt% water in the solution was needed for PS(25)-P4VP(7) whereas 10 wt% water was enough for PS(51)-P4VP(18). The non-polar PS patches in the colloidal monomer generate the attraction necessary for polymerization of the colloidal monomers, which is originated to avoid unfavorable contacts of the PS patches with the polar solvent containing water. Thus, a larger patch of the PS block can induce stronger attraction, i.e., higher reactivity of the colloidal monomer. Therefore, the colloidal monomer of PS(51)-P4VP(18) having larger PS patches can be polymerized with a lower content of water. In addition, the colloidal monomers of PS(51)-P4VP(18) produced a higher degree of polymerization (approximately 262 by dividing the chain length of ~8.9 μm with the monomer length of ~34 nm) than those of PS(25)-P4VP(7) (~117 by ~2.8 μm ÷ ~24 nm) after 48 hr polymerization (Figures 2.3 and 2.8), indicating faster polymerization with larger PS patches. It is noted that polymerization of colloidal monomers in the condition we used was relatively slow because 24 hr or longer polymerization was necessary to detect a supracolloidal chain with an appreciable length. We also note that aggregation of the colloidal monomers was observed in low contents of water after 48 hr, presumably because low contents of water would not generate enough repulsion between the P4VP

cores, which were directly exposed to the solvent, to avoid the lateral aggregation of colloidal monomers (Figure 2.9). A study on the detail of polymerization of colloidal monomers depending on water contents and non-polar patch sizes is in progress.

We had two different colloidal monomers of PS(51)-P4VP(18) and PS(25)-P4VP(7) that were well discernible in TEM images due to their sizes. Thus, we demonstrated the synthesis of supracolloidal random and block copolymer chains. For random copolymerization, two colloidal monomers of PS(51)-P4VP(18) and PS(25)-P4VP(7) after DMF addition were first mixed and then polymerized by water addition. Figure 2.10a shows a supracolloidal random copolymer consisting of the colloidal monomers of PS(51)-P4VP(18) and PS(25)-P4VP(7) whose cores are marked by green and pink false colors, respectively. A whole chain of the random copolymer is shown in the inset and clearly visible in an enlarged image of Figure 2.11. We mixed two colloidal monomers with the same weight so that the number of small colloidal monomers of PS(25)-P4VP(7) were 2.8 times more than that of large monomers of PS(51)-P4VP(18) in an initial monomer solution by considering the volume ratio of large to small micelles equal to 2.8 which was estimated from the TEM images. Although counting of the monomer units in the chain (Figure 2.11) was statistically insufficient, the small monomer units in the random copolymer were found 1.8 times more than the large monomer units. In addition, the chain length of random copolymers was similar to that of the homopolymer of small colloidal monomers, presumably because prevalent small

colloidal monomers, which are less reactive, could govern the growth of the chain.

We also synthesized a supracolloidal block copolymer simply by mixing two pre-polymerized chains. We first synthesized two homopolymer chains of the colloidal monomers of PS(51)-P4VP(18) and PS(25)-P4VP(7) for 24 hr polymerization. Then, two homopolymers were mixed with the same weight for additional 24 hr. Figure 2.10b clearly shows a supracolloidal block copolymer chain consisting of two end blocks of PS(25)-P4VP(7) in pink color and one middle block of PS(51)-P4VP(18) in green color. An enlarged image is also given in Figure 2.12. We note that more homopolymer chains of PS(25)-P4VP(7) were added for block copolymerization because of mixing in the same weight of two pre-polymer chains. It is also noted that the length of each block in the block copolymer was relatively short because homopolymer chains were polymerized only for 24 hr.

2.4. Conclusions

Based on the concept of directional attraction with orthogonal repulsion to the attraction between colloidal building blocks to achieve a linear assembly of colloidal nanoparticles, we accomplished supracolloidal polymerization of colloidal monomers of PS-P4VP diblock copolymers. We induced colloidal monomers of PS-P4VP micelles with the non-polar PS patches in the corona and the cross-linked P4VP core directly exposed to the solvent. During the polymerization of these colloidal monomers driven by increasing the polarity of the solvent, the non-polar PS patches worked as attractive parts for the reaction whereas the exposed polar P4VP core acted as a repulsive part to limit non-directional aggregation so that a supracolloidal polymer was synthesized. Because the size of colloidal monomers was determined by the molecular weight of PS-P4VP, we were able to synthesize supracolloidal random and block copolymers consisting of large and small colloidal monomers. The strategy demonstrated here is applicable to various diblock copolymers which can form a micelle with a cross-linkable core so that we expect a variety of supracolloid polymer chains with diverse colloidal building blocks. In addition, encapsulation of functional materials such as quantum dots, metal nanoparticles, and fluorophores into the core of diblock copolymer micelles[30] is feasible so that supracolloidal polymers of diblock copolymer micelles can be further functionalized for numerous applications.

2.5. References

[1] F. Li, D. P. Josephson, A. Stein, *Angew. Chem. Int. Ed.* **2011**, *50*, 360.

[2] M. Grzelczak, J. Vermant, E. M. Furst, L. M. Liz-Marzán, *ACS Nano* **2010**, *4*, 3591.

[3] E. V. Shevchenko, D. V. Talapin, N. A. Kotov, S. O'Brien, C. B. Murray, *Nature* **2006**, *439*, 55.

[4] Z. Nie, A. Petukhova, E. Kumacheva, *Nat. Nanotechnol.* **2010**, *5*, 15.

[5] J. Pyun, *Angew. Chem. Int. Ed.* **2012**, *51*, 12408.

[6] L. J. Hill, N. Pinna, K. Char, J. Pyun, *Prog. Polym. Sci.* **2014**, DOI: 10.1016/j.progpolymsci.2014.08.003.

[7] Z. Nie, D. Fava, E. Kumacheva, S. Zou, G. C. Walker and M. Rubinstein, *Nat. Mater.* **2007**, ***6***, 609.

[8] Z. Nie, D. Fava, M. Rubinstein, E. Kumacheva, *J. Am. Chem. Soc.* **2008**, *130*, 3683.

[9] R. M. Choueiri, A. Klinkova, J. Thérien-Aubin, M. Rubinstein, E. Kumacheva, *J. Am. Chem. Soc.* **2013**, *135*, 10262.

[10] J. Lai, Y. Xu, X. Mu, X. Wu, C. Li, J. Zheng, C. Wu, J. Chen, Y. Zhao, *Chem. Commun.* **2011**, *47*, 3822.

[11] S. Boissé, J. Rieger, K. Belal, A. Di-Cicco, P. Beaunier, M. H. Li, B. Charleux, *Chem. Commun.* **2010**, *46*, 1950.

[12] A. Blanazs, R. Verber, O. O. Mykhaylyk, A. J. Ryan, J. Z. Heath, C. W. I. Douglas, S. P. Armes, *J. Am. Chem. Soc.* **2012**, *134*, 9741.

[13] L. A. Fielding, J. A. Lane, M. J. Derry, O. O. Mykhaylyk, S. P. Armes, *J. Am. Chem. Soc.* **2014**, *136*, 5790.

[14] Z. Jia, V. A. Bobrin, N. P. Truong, M. Gillard, M. J. Monteiro, *J. Am. Chem. Soc.* **2014**, *136*, 5824.

[15] Y. Y. Won, H. T. Davis, F. S. Bates, *Science* **1999**, *283*, 960.

[16] G. Liu, L. Qiao, A. Guo, *Macromolecules* **1996**, *29*, 5508.

[17] Z. Li, E. Kesselman, Y. Talmon, M. A. Hillmyer, T. P. Lodge, *Science* **2004**, *306*, 98.

[18] J. Zhu, S. Zhang, F. Zhang, K. L. Wooley, D. J. Pochan, *Adv. Funct. Mater.* **2013**, *23*, 1767.

[19] Z. M. Hudson, D. H. Lunn, N. A. Winnik, I. Manners, *Nat. Commun.* **2014**, *4*, 3372.

[20]K. Y. Yoon, I. H. Lee, K. O. Kim, J. Jang, E. Lee, T. L. Choi, *J. Am. Chem. Soc.* **2012**, *134*, 14291.

[21] A. H. Gröschel, F. H. Schacher, H. Schmalz, O. V. Borisov, Ekaterina B. Zhulina, A. Walther, A. H. E. Müller, *Nat. Commun*. **2012**, *3*, 710.

[22] A. H. Gröschel, A. Walther, T. I. Löbling, F. H. Schacher, H. Schmalz, A. H. E. Müller, *Nature* **2013**, *503*, 247.

[23] G. Casalborn-Miceli, A. Zanelli, A. W. Rinaldi, E. M. Girotto, M. J. Yang, Y. S. Chen, Y. Li, *Langmuir* **2005**, *21*, 9704.

[24] W. Lee, S. Y. Lee, R. M. Briber, O. Rabin, *Adv. Funct. Mater.* **2011**, *21*, 3424.

[25] K. S. Kim, J. H. Kim, H. Kim, F. Laquai, E. Arifin, J. K. Lee, S. I. Yoo, B. H. Sohn, *ACS Nano* **2012**, *6*, 5051.

[26] H. Lee, K. Char, *ACS Appl. Mater. Inter.* **2009**, *1*, 913.

[27] J. Brandrup, E. H. Immergut, E. A. Grulke, A. Abe, D. R. Bloch, in *Polymer Handbook*, Wiley-Interscience, New York, 4th ed., **1999**.

[28] S. Park, J. Y. Wang, B. Kim, W. Chen, T. P. Russell, *Macromolecules* **2007**, *40*, 9059.

[29] L. A. Fielding, M. J. Derry, V. Ladmiral, J. Rosselgong, A. M. Rodrigues, L. P. D. Ratcliffe, S. Sugihara, S. P. Armes, *Chem. Sci.* **2013**, *4*, 2081.

[30] S. I. Yoo, S. J. An, G. H, Choi, K. S. Kim, G. C. Yi, W. C. Zin, J. C. Jung, B. H. Sohn, *Adv. Mater.* **2007**, *19*, 1594.

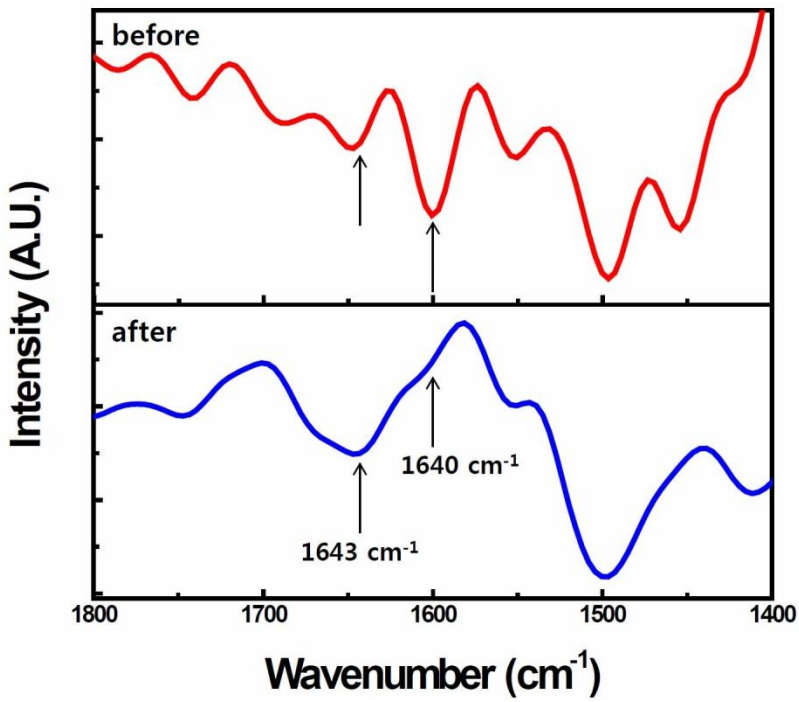

Figure 2.1. FT-IR spectra of PS(51)-P4VP(18) micelles before and after cross-linking by DBB with a molar ratios of DBB to 4VP equal to 0.5. The bands at 1600 cm^{-1} and 1643 cm^{-1} correspond to 4VP and quaternized 4VP, respectively.

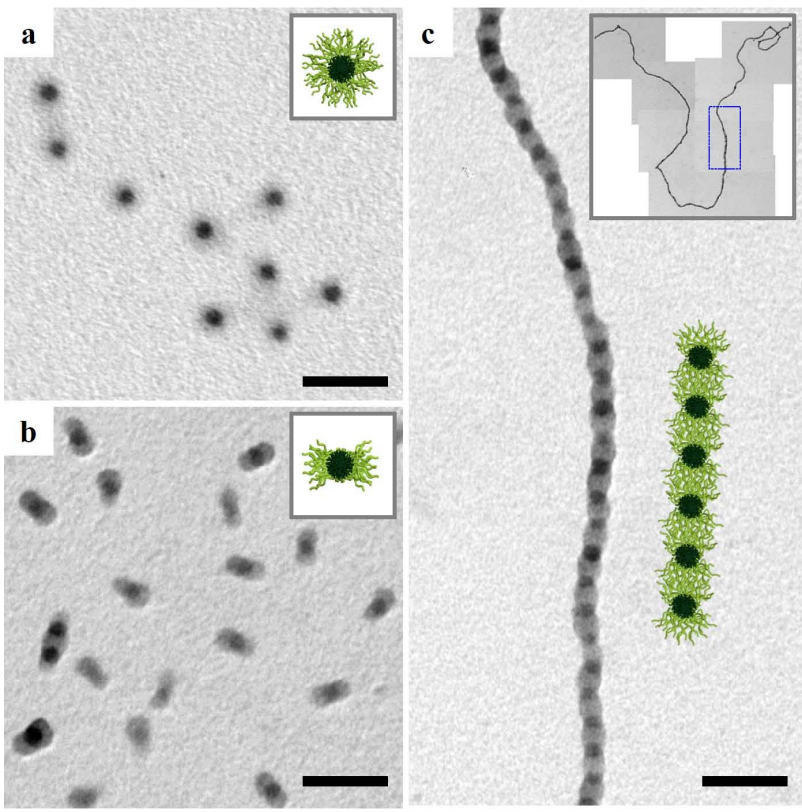

Figure 2.2. TEM images: (a) spherical micelles of PS(51)-P4VP(18); (b) micellar colloidal monomers; (c) a supracolloidal polymer chain. All scale bars are 100 nm. The image in (c) corresponds to the marked area in the inset (3 μm × 3 μm) which shows a whole chain.

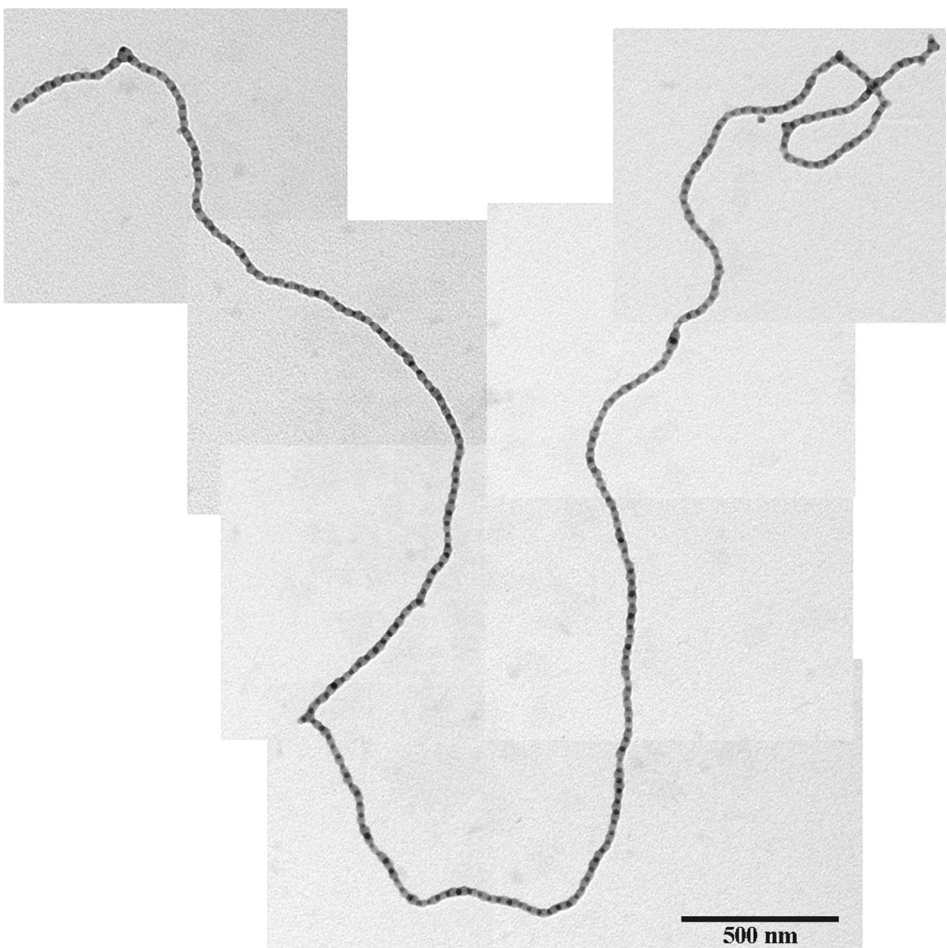

Figure 2.3. TEM image of a supracolloidal polymer chain of PS(51)-P4VP(18) colloidal monomers shown in the inset of Figure 2.2c.

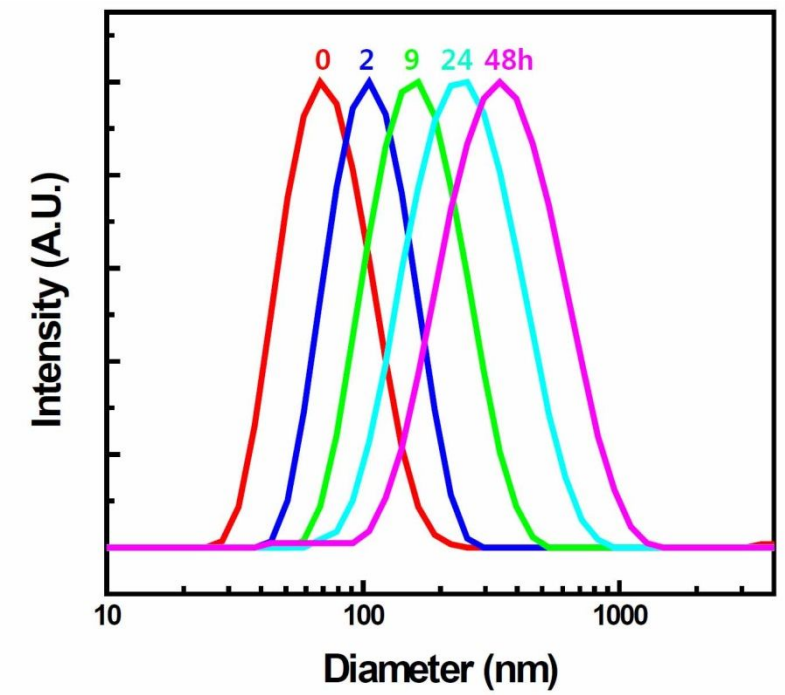

Figure 2.4. A change of colloidal diameters as polymerization of PS(51)-P4VP(18) colloidal monomers by DLS measurements. The maximum intensities after 0, 2, 9, 24, and 48 hr correspond to the diameters of 77, 112, 174, 269, and 387 nm, respectively.

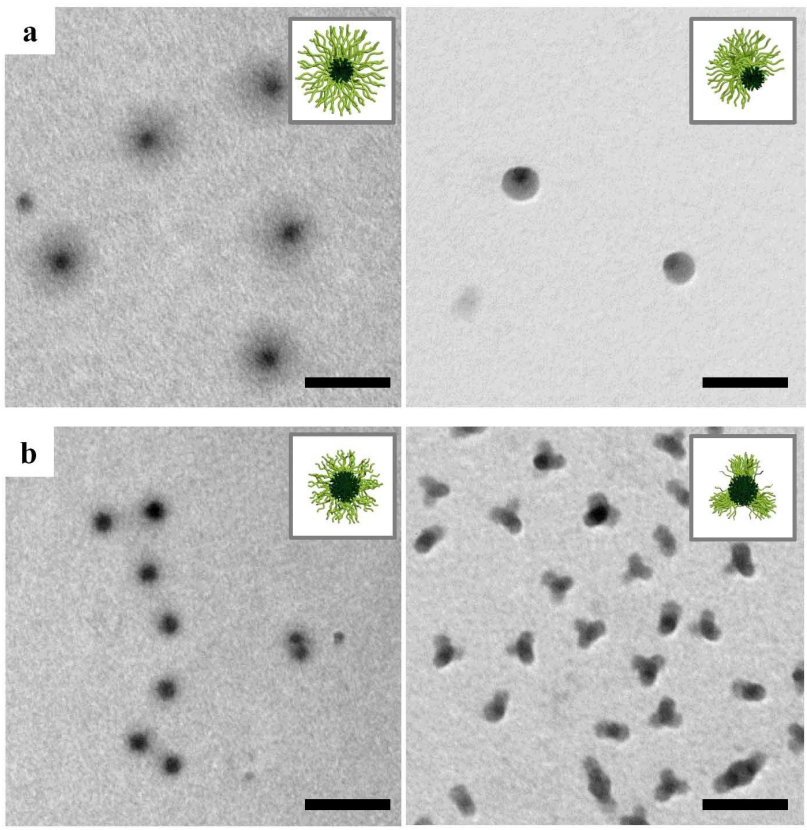

Figure 2.5. TEM images of spherical micelles of PS-P4VP (left) and rearranged micellar colloids (right): (a) PS(109)-P4VP(27); (b) PS(41)-P4VP(24). All scale bars are 100 nm.

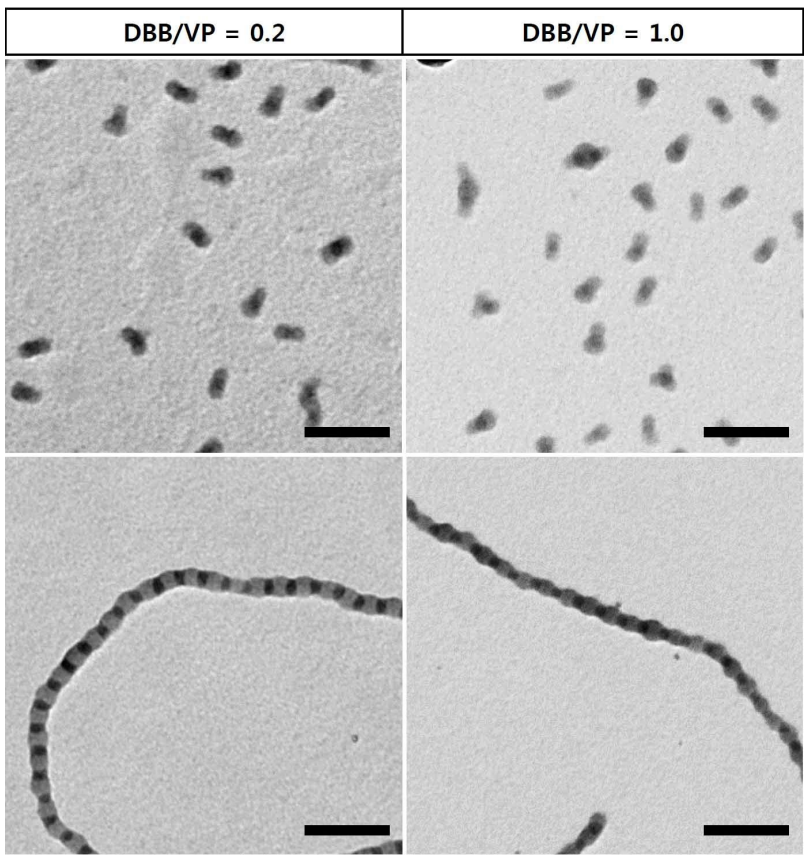

Figure 2.6. TEM images of rearranged micellar colloids (top) and supracolloidal polymers (bottom) of PS(51)-P4VP(18) depending on the molar ratio of DBB to 4VP; 0.2 (left column) and 1.0 (right column).

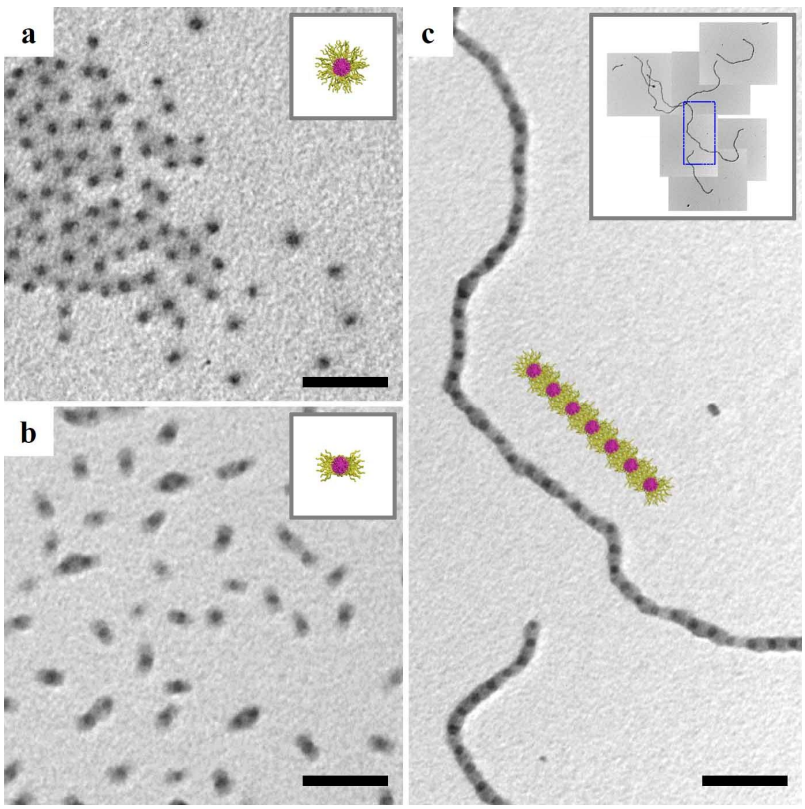

Figure 2.7. TEM images: (a) spherical micelles of PS(25)-P4VP(7); (b) colloidal monomers; (c) a supracolloidal polymer chain. All scale bars are 100 nm. The image in (c) corresponds to the marked area in the inset (3 μm × 3 μm) which shows several whole chains.

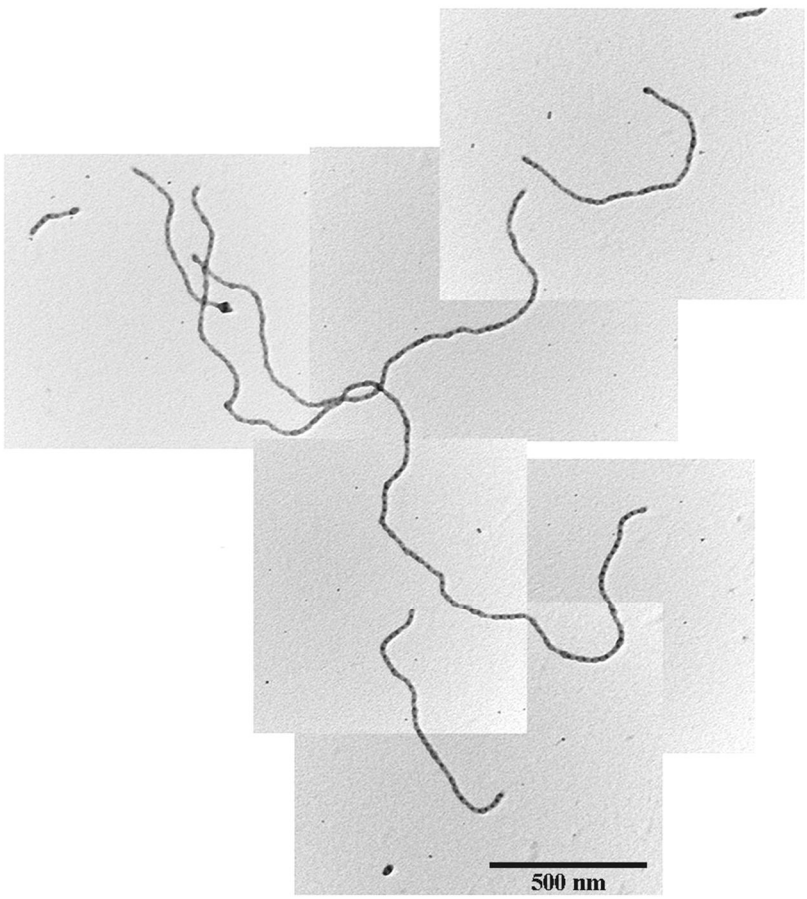

Figure 2.8. TEM image of supracolloidal polymer chains of PS(25)-P4VP(7) colloidal monomers shown in the inset of Figure 2.7c.

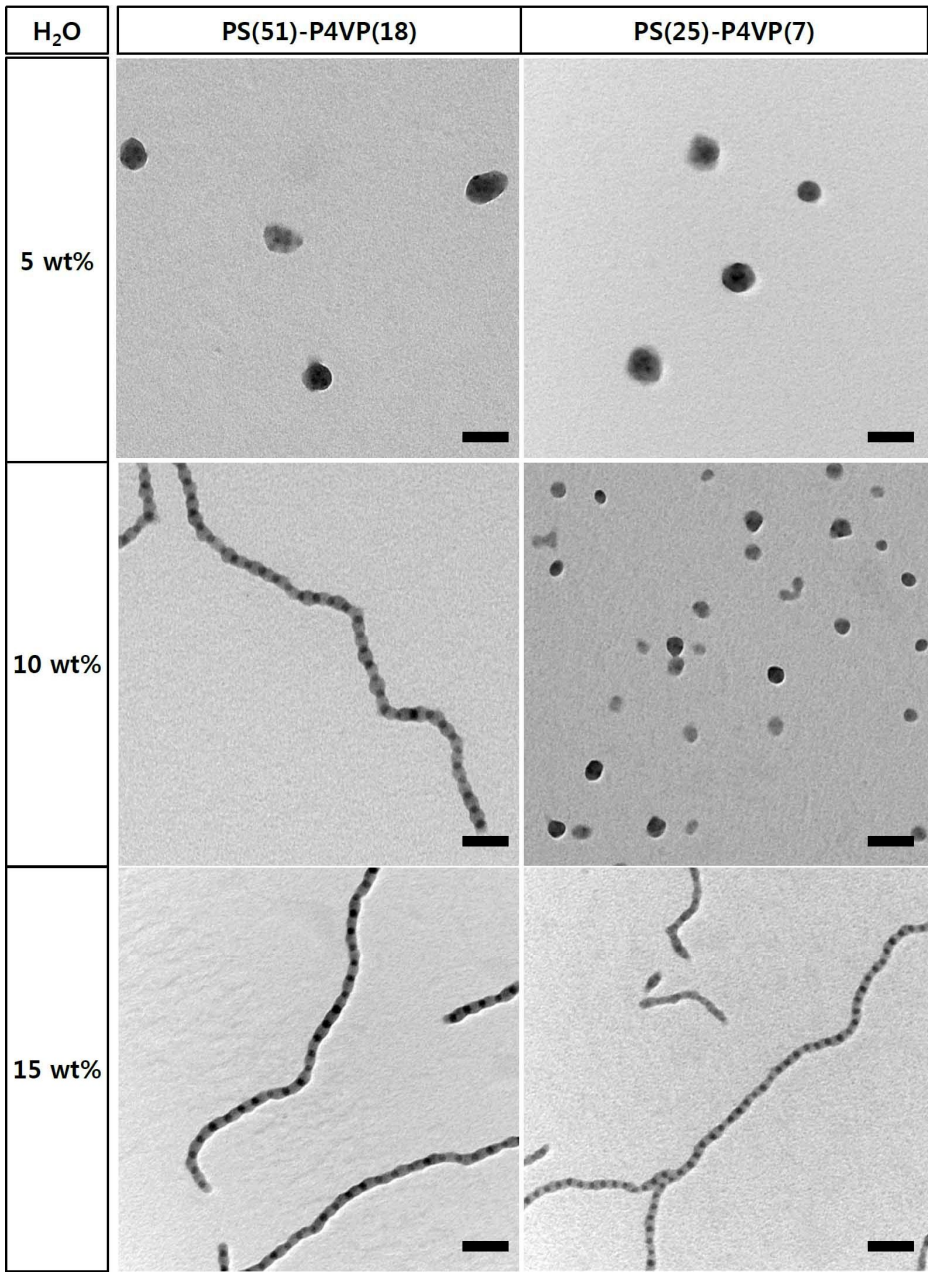

Figure 2.9. TEM images of supracolloidal assemblies of colloidal monomers of PS(51)-P4VP(18) (left column) and colloidal monomers of PS(25)-P4VP(7) (right column) depending on H_2O contents. All scale bars are 100 nm.

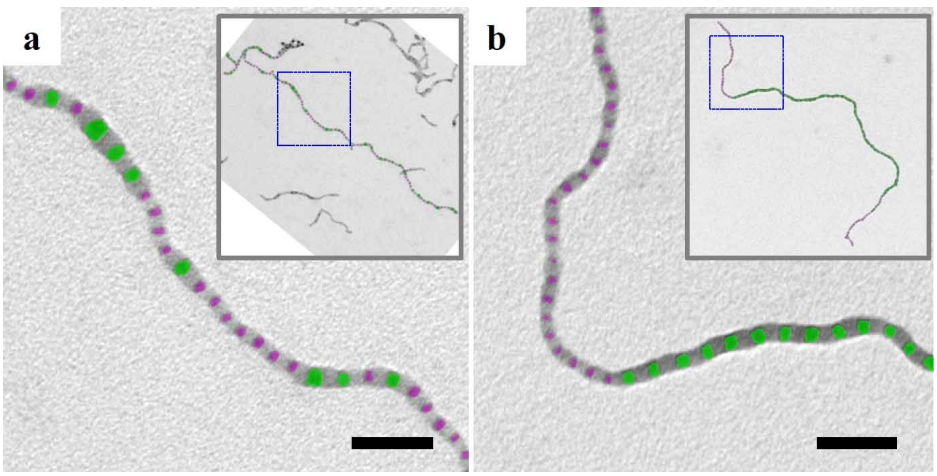

Figure 2.10. TEM images of supracolloidal copolymer chains; (a) random copolymer; (b) block copolymer. The scale bars are 100 nm. Each image corresponds to the marked area in the inset (2 μm × 2 μm). Green and pink false colors are applied to the cores of PS(51)-P4VP(18) and PS(25)-P4VP(7), respectively.

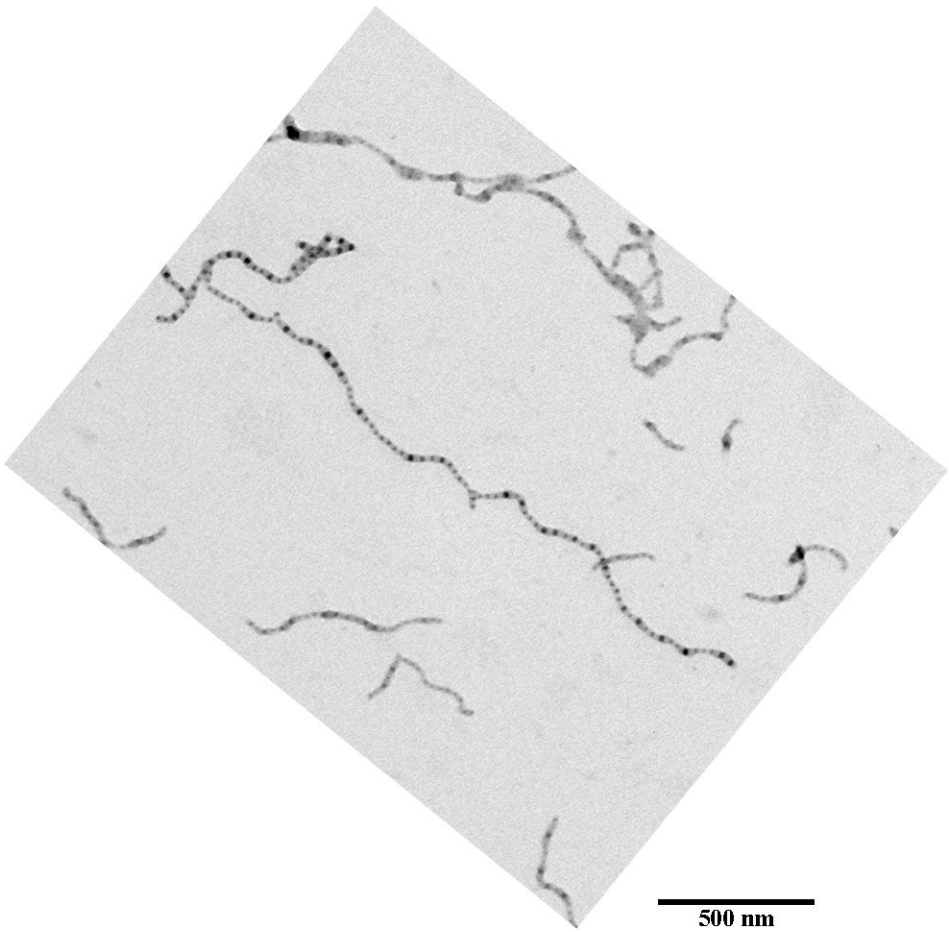

Figure 2.11. TEM image of supracolloidal random copolymer chains shown in the inset of Figure 2.10a.

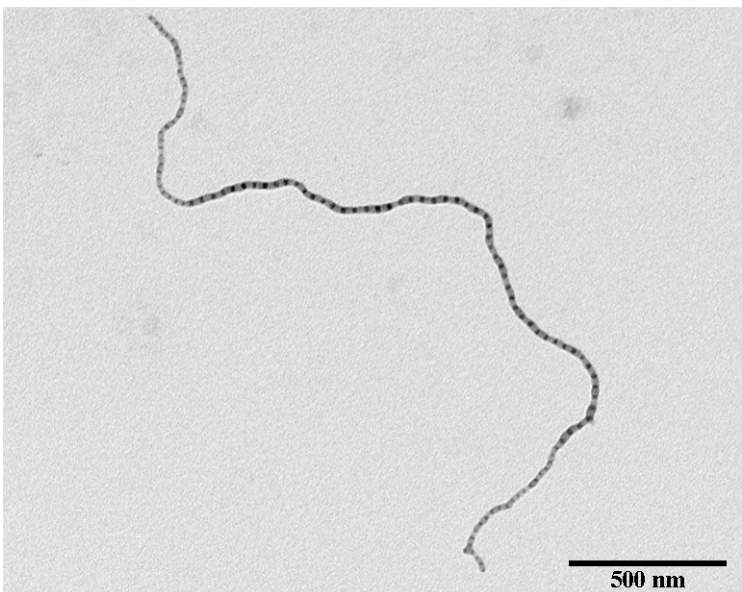

Figure 2.12. TEM image of a supracolloidal block copolymer chain shown in the inset of Figure 2.10b.

Chapter 3

Inversion of Block Copolymer Micelles for Conversion of Gold Nanoparticle Patterns

3.1. Introduction

Nanoparticles of metals and semiconductors have unique optical, electronic, and chemical properties which cannot be observed in their bulk counterparts.[1,2] For example, metallic nanoparticles have absorption bands at specific wavelengths due to their surface plasmon resonances.[3] Optical characteristics of metallic nanoparticles depend on the size, shape, and inter-particle distance, which should be controlled for various applications including photonic devices and biosensors, particularly on solid substrates.[3,4] The e-beam lithography can provide the ultimate generation of periodic nanostructures, with regular shapes and sizes in well-controlled manners, which can be considered as perfect arrangement of nanoparticles.[5,6] However, low throughputs and high costs due to the serial nature of the e-beam lithography should be overcome for efficient creation of nanostructures in large area.[7]

A bottom-up self-assembling approach can effectively produce nanostructures of various materials with controlled shapes, sizes, and inter-particle distances in large area.[8] Especially, diblock copolymers, which form self-assembled nanodomains, can be utilized as valuable nanotemplates for fabrication of nanostructures of a variety of materials in a controlled manner.[9,10] For example, metallic patterns of nanodots and nanolines can be easily produced by spherical,[11-13] cylindrical,[14-17] or lamellar nanodomains[18,19] of diblock copolymers. We also demonstrated a highly ordered two-dimensional array of gold nanoparticles using a hexagonal array of diblock copolymer micelles as a

successful template.[20] Furthermore, nanostructures of diblock copolymers allow the synthesis and arrangement of nanoparticles with unusual shapes such as rings and donuts.[21-23] For instance, toroidal micelles of diblock copolymers were applied to the production of gold nanorings having the highly uniform size and shape.[21] An array of metallic nanorings was recently demonstrated by reconstructing the morphology of diblock copolymer micelles in thin films with selective swelling of the core blocks.[22] We also employed a donut-like nanostructure in a thin film of triblock copolymers as a template to produce metallic nanorings.[24]

In this chapter, we first synthesized a diblock copolymer, consisting of one block which allows the synthesis of nanoparticles and the other block which is selectively removable, by the reversible addition-fragmentation chain transfer (RAFT) polymerization. Using a selective solvent for each block, we produced two types of spherical micelles, which have the inversed position of two blocks, that is, the core of the nanoparticle-synthesizable block and the corona of the removable block, and vice versa. Then, we coated single layers of these two micelles on substrates, which were successfully employed as templates for the synthesis and arrangement of spherical gold nanoparticles and their ring-like configuration in large area.

3.2. Experimental Section

PMMA-P2VP diblock copolymer

Poly(methylmethacrylate)-poly(2-vinylpyridine), PMMA-b-P2VP, diblock copolymers were synthesized by the reversible addition-fragmentation chain transfer (RAFT) polymerization.[25,26] Azobisisobutyronitrile (AIBN) and cumyldithiobenzoate were used as an initiator and a chain transfer agent (CTA), respectively. Cumyldithiobenzoate was synthesized according to the literatures.[27,28] MMA and 2VP monomers were distilled under reduced pressure. 13 g (0.13 mol) of MMA, 51 mg (0.18 mmol) of cumyldithiobenzoate, and 3.7 mg (0.0023 mmol) of AIBN were added to 8 ml of distilled benzene, and then air was exchanged with argon by three freeze-thaw cycles. Polymerization of MMA was carried out at 75 ℃ for 48 hr. Polymers were purified by precipitating them into cold ethanol. Two more precipitations were performed from their THF solutions. After drying at 30 ℃ for 4 hr in vacuum, 10 g (77%) of PMMA was obtained in pink powders. The number average molecular weight is 41,000 g mol^{-1} and the dispersity index is 1.09 (figure 3.1). Then, 2.6 g (0.0064 mmol) of PMMA, which can act as macro-CTA,[29] was dissolved in 4 mL of DMF. 2.6 mg (0.0016mmol) of AIBN and 6.0 g (0.057 mmol) of 2VP, a monomer for the second block, were added. The whole mixture was heated to 70 ℃ under argon and polymerization was carried out for 24 hr. Products were dissolved into THF and purified by precipitating them into a mixture of ethanol and water (4 : 6). After drying at 30 ℃ for overnight in vacuum, PMMA-b-P2VP in pale pink powders were obtained. The

weights ratio between PMMA blocks and P2VP blocks were 2 : 1 (figure 3.2) and the dispersity index is 1.20 (figure 3.1).

Nanostructures of PMMA-P2VP micelles and Au nanoparticles

The fabrication procedures of nanostructures and Au nanoparticles using PMMA-b-P2VP micelles are illustrated in Figure 3.3. Two different types of PMMA-b-P2VP micelles were prepared using toluene, a selective solvent for the PMMA block, and isopropanol, a selective solvent for the P2VP block. For P2VP(core)-PMMA(corona) micelles, PMMA-b-P2VP copolymers were dissolved in toluene at 80 ℃ and then the solution was cooled down to room temperature to yield a 0.5 wt% solution. A 0.1 wt% PMMA(core)-P2VP(corona) micellar solution was also prepared by dissolving PMMA-b-P2VP in isopropanol. When the copolymer was added to isopropanol, the solution was not transparent at room temperature. After heating the solution at 100 ℃ in a sealed container and cooling to room temperature, it became a clear solution. From these micellar solutions, single layers of P2VP(core)-PMMA(corona) micelles and PMMA(core)-P2VP(corona) micelles were spin-coated onto silicon wafers at 2000 rpm for 1 min. Selective removal of the PMMA block of PMMA-b-P2VP copolymers was conducted by UV irradiation (325 nm, 15 W) for 1 hr, followed by washing with toluene.[30,31] For selective incorporation of gold precursors into the P2VP blocks, spin-coated PMMA-b-P2VP micelles were immersed into a 10 mM ethanol solution of $HAuCl_4$ for 5 ~ 10 min and then thoroughly rinsed with ethanol.[32]

After the removal of PMMA blocks of PMMA-b-P2VP micelles containing gold precursors, oxygen plasma (100 W, 3.8×10^{-2} Torr, 10 min) was carried out to synthesize Au nanoparticles with complete removal of copolymers.[33,34]

Characterization

NMR spectra were obtained on a Varian NMR System (500 MHz). Gel permeation chromatography (GPC) was carried out on a Waters system (1515 pump, 2414 refractive index detector) with a Shodex GPC LF-804 column. Surface morphologies of micellar nanostructures and gold nanoparticles were investigated by atomic force microscopy (AFM, Nanoscope IIIA, Digital Instrument) in tapping mode with Al-coated Si cantilevers. Transmission electron microscopy (TEM) analysis was performed on a Hitachi 7600 operating at 100 kV for diblock copolymer micelles and JEM-2100 (JEOL) operating at 200 kV for Au nanoparticles.

3.3. Results and Discussion

In toluene, a selective solvent for the PMMA block, PMMA-b-P2VP copolymers assemble into P2VP(core)-PMMA(corona) micelles as shown in Figure 3.3a. A height-mode AFM image of P2VP(core)-PMMA(corona) micelles coated on a silicon wafer is shown in Figure 3.4a, in which the bright spheres correspond to the copolymer micelles. The shape of the micelles is somewhat irregular but mostly spherical. The spherical micelles can be also found in the TEM image given in the inset. We note that the TEM image was obtained without staining so that it shows an entire micelle. The micelles were organized into a single layer in close-packed arrangement without the indication of multilayers. Thus, we confirmed that P2VP(core)-PMMA(corona) micelles can be arranged in a single layer as like P2VP(core)-PS(corona) micelles and P4VP(core)-PS(corona) micelles,[20,33] although the shape and ordering of micelles were rather deteriorated. Organization of P2VP(core)-PMMA(corona) micelles can be also analyzed from a height profile drawn along the white line in the image. The center-to-center distance between the micelles is ~58 nm, indicating the micellar diameter of ~29 nm. This value would be much smaller than that of the micelles in a solution because the PMMA corona of the micelles shrank and overlapped each other in the close-packed arrangement of the solid layer after fast evaporation of the solvent by spin coating.[35] The height of the micelles in the height profile is only ~4.5 nm, which is much smaller than the diameter of the micelles because this value merely measures the distance from the position of the micellar overlap to the top of the

micellar center.

The PMMA block of P2VP-PMMA copolymers can be selectively removed by UV irradiation.[30] As illustrated in Figure 3.3a, the PMMA coronas in the single layer of P2VP(core)-PMMA(corona) micelles in Figure 3.4a were removed by UV exposure followed by washing with toluene. Figure 3.4b shows an AFM image of the nanostructures obtained after selective removal of PMMA coronas, which are similar to the micellar nanostructures before the corona removal (Figure 3.4a) without serious changes in shape and size. In the height profile, the distance between the nanostructures was maintained as ~58 nm, indicating that the center-to-center distance between the micelles was not changed after removal of PMMA coronas. The peak height (~5.5 nm) is also similar to that before the corona removal shown in Figure 3.4a, presumably because the selective removal of the PMMA coronas which covered all the surface of the overlapped micelles in the single layer would not change the distance from the micellar overlap to the top of the micellar center.

PMMA-b-P2VP copolymers also assemble into PMMA(core)-P2VP(corona) micelles in isopropanol which is a selective solvent for the P2VP block (Figure 3.3b). These PMMA(core)-P2VP(corona) micelles can be coated on substrates by spin coating which allows fast solvent evaporation. The AFM image of Figure 3.5a shows spherical PMMA(core)-P2VP(corona) micelles coated on a silicon wafer. The spherical micelles can be also found in the TEM image given in the inset. Unlike the close-packed P2VP(core)-PMMA(corona) micelles in Figure 3.4a,

PMMA(core)-P2VP(corona) micelles are separated from each other without overlapping because a low concentration of the micellar solution was employed.[36] As shown in Figure 3.5a, the size distribution of the micelles is rather broad. The diameter of two micelles in the height profile is ~60 nm, which is larger than that of P2VP(core)-PMMA(corona) micelles. The height of the micelles is ~28 nm, which can be the total thickness of the micelle because these micelles did not overlap each other. Since the thickness of the micelle is smaller than its diameter, the micelle is essentially flattened on the substrate.[37]

To remove the PMMA cores selectively, PMMA(core)-P2VP(corona) micelles in Figure 3.5a were treated by UV irradiation followed by washing with toluene as explained in the schematic of Figure 3.3b. In the AFM image of Figure 3.5b, we can find donut-like nanostructures after selective removal of the PMMA cores, which are clearly visible in the TEM image given in the inset. Regardless of the micellar sizes, donut-like nanostructures were produced, in which the central part is lower than the peripherals. From two nanostructures in the height profile, the outer diameter of donut-like structures is ~80 nm, which is slightly larger than the diameter of the micelles before the PMMA removal. Furthermore, the height of donut-like nanostructures is only ~7 nm, which is much smaller than that of the untreated micelles. In addition, the height at the central part of the nanostructures is ~4 nm. This finite thickness at the center indicates that the central part is not empty, implying that the nanostructure can be more closely described as a crater-like structure. This unique nanostructure would be created by the collapse of the P2VP

coronas after the removal of the PMMA core which generates the pore at the core of the micelle.[38] From the results demonstrated in Figures 3.4 and 3.5, we confirmed that two types of PMMA-b-P2VP micelles which have the inversed position of two blocks can be obtained by selective solvents and further converted to spherical or donut-like nanostructures by selective removal of the PMMA block.

As illustrated in Figure 3.3, $HAuCl_4$, a precursor of gold nanoparticles, was selectively incorporated into the P2VP cores or coronas of PMMA-b-P2VP micelles. Subsequently the PMMA coronas or cores were selectively removed by UV irradiation and toluene washing. Then, oxygen plasma treatment was conducted for synthesis of gold nanoparticles and complete removal of copolymers. Figure 3.6a is an AFM image of gold nanoparticles synthesized from a single layer of P2VP(core)-PMMA(corona) micelles shown in Figure 3.4a, in which gold nanoparticles with the diameter of ~28 nm were uniformly coated on the substrate. The TEM image given in the inset also clearly shows a spherical gold nanoparticle. Thus, we confirmed that a single layer of P2VP(core)-PMMA(corona) micelles can be a template for the synthesis of gold nanoparticles as that of P2VP(core)-PS(corona) micelles or P4VP(core)-PS(corona) micelles.[20,33]

In sharp contrast to the synthesis of gold nanoparticles from P2VP(core)-PMMA(corona) micelles, ring-like arrangement of gold nanoparticles was obtained from PMMA(core)-P2VP(corona) micelles. In the AFM image of Figure 3.6b, we can find that gold nanoparticles are arranged in ring configuration. The diameter of gold nanoparticles synthesized is ~21 nm. The TEM image also clearly shows a

spherical gold nanoparticle. As shown in Figure 3.5b, donut-like nanostructures of P2VP blocks can be formed by selective removal of the PMMA cores of PMMA(core)-P2VP(corona) micelles, which would guide the formation of gold nanoparticles in ring-like arrangement. Therefore, we were able to fabricate not only typical arrangement of spherical gold nanoparticles but also their ring-like configuration from single layers of two types of PMMA-b-P2VP micelles which have the inversed position of the core and the corona.

3.4. Conclusions

We synthesized PMMA-b-P2VP copolymers consisting of the removable PMMA block and the nanoparticle-synthesizable P2VP block, from which P2VP(core)-PMMA(corona) micelles and PMMA(core)-P2VP(corona) micelles were fabricated and coated on the solid substrate using toluene and isopropanol as a selective solvent for the PMMA and the P2VP block, respectively. Then, we were able to create spherical and donut-like nanostructures from single layers of these micelles, which have the inversed position of the core and the corona, by selective removal of the PMMA coronas or cores. These nanostructures were further employed as templates for the synthesis and arrangement of spherical gold nanoparticles and their ring-like configuration in large area. Since a variety of nanoparticles with a controlled inter-particle distance can be synthesized using diblock copolymer micelles as templates,[9] the demonstration here can extend the applicability of diblock copolymer micelles for the effective synthesis and arrangement of nanoparticles.

3.5. References

[1] E. Hutter, J. H. Fendler, *Adv. Mater.* **2004**, *16*, 1685.

[2] W. J. Parak, D. Gerion, T. Pellegrino, D. Zanchet, C. Micheel, S. C. Williams, R. Boudreau, M. A. Le Gros, C. A. Larabel, A. P. Alivisatos, *Nanotechnology* **2003**, *14*, R15.

[3] J. N. Anker, W. P. Hall, O. Lyandres, N. C. Shah, J. Zhao, R. P. van Duyne, *Nat. Mater.* **2008**, *7*, 442.

[4] X. Huang, S. Neretina, M. A. El-Sayed, *Adv. Mater.* **2009**, *21*, 4880.

[5] K. H. Su, Q. H. Wei, J. J. Mock, D. R. Smith, S. Schultz, X. Zhang, *NanoLett.* **2003**, *3*, 1087.

[6] P. P. Pompa, L. Martiradonna, A. Della Torre, F. Della Sala, L. Manna, M. De Vittorio, F. Calabi, R. Cingolani, R. Rinaldi, *Nat. Nanotechnol.* **2006**, *1*, 126.

[7] R. A. Segalman, *Mater. Sci. Eng. R Rep.* **2005**, *48*, 191.

[8] J. Zhang, Y. Li, X. Zhang, B. Yang, *Adv. Mater.* **2010**, *22*, 4249.

[9] C. Park, J. Yoon, E. L. Thomas, *Polymer* **2003**, *44*, 6725.

[10] S. Forster, M. Antonietti, *Adv. Mater.* **1998**, *10*, 195.

[11] J. P. Spatz, S. Mossmer, C. Hartmann, M. Moller, T. Herzog, M. Krieger, H. Boyen, P. Ziemann, B. Kabius, *Langmuir* **2000**, *16*, 407.

[12] X. Li, K. H. A. Lau, D. H. Kim, W. Knoll, *Langmuir* **2005**, *21*, 5212.

[13] S. I. Yoo, J. H. Kwon and B. H. Sohn, *J. Mater. Chem.* **2007**, *17*, 2969.

[14] J. Chai, D. Wang, X. Fan, J. M. Buriak, *Nat. Nanotechnol.* **2007**, *2*, 500.

[15] V. Gowrishankar, N. Miller, M. D. McGehee, M. J. Misner, D. Y. Ryu, T. P.

Russell, E. Drockenmuller, C. J. Hawker, *Thin Solid Films* **2006**, *513*, 289.

[16] Y. S. Jung, C. A. Ross, *NanoLett.* **2007**, *7*, 2046.

[17] O. Seifarth, R. Krenek, I. Tokarev, Y. Burkove, A. Sidorenko, S. Minko, M. Stamm, D. Schmeisser, *Thin Solid Films* **2007**, *515*, 6552.

[18] S. M. Park, M. P. Stoykovich, R. Ruiz, Y. Zhang, C. T. Black, P. F. Nealey, *Adv. Mater.* **2007**, *19*, 607.

[19] G. Xia, S. J. Jeong, J. E. Kim, B. H. Kim, C. M. Koo, S. O. Kim, *Nanotechnology* **2009**, *20*, 225301.

[20] S. H. Yun, S. I. Yoo, J. C. Jung, W. C. Zin, B. H. Sohn, *Chem. Mater.* **2006**, *18*, 5646.

[21] H. Huang, B. Chung, J. Jung, H. W. Park, T. Chang, *Angew. Chem. Int. Ed.* **2009**, *48*, 4594.

[22] X. Zu, X. Hu, L. A. Lyon, Y. Deng, *Chem. Commun.* **2010**, *46*, 7927.

[23] S. Park. J. Y. Wang, B. Kim, T. P. Russell, *NanoLett.* **2008**, *8*, 1667.

[24] S. M. Jeon, K. Y. Jang, S. H. Lee, H. W. Park, B. H. Sohn, *Langmuir* **2008**, *24*, 11137.

[25] G. Moad, E. Rizzardo, S. H. Thang, *Aust. J. Chem.* **2005**, *58*, 379.

[26] P. J. Roth, K. T. Wiss, R. Zentel, P. Theato, *Macromolecules* **2010**, *41*, 8513.

[27] M. Eberhardt, R. Mruk, R. Zentel, P. Theato, *Eur. Polym.J.* **2005**, *41*, 1569.

[28] J. Chiefari, Y. K. Chong, F. Ercole, J. Jeffery, T. P. T. Le, R. T. A. Mayadunne, G. F. Meijs, C. L. Moad, G. Moad, E. Rizzardo, S. H. Thang, *Macromolecules* **1998**, *31*, 5559.

[29] Y. K. Chong, T. P. T. Le, G. Moad, E. Rizzardo, S. H. Thang, *Macromolecules* **1999**, *32*, 2071.

[30] T. Thurn-Albrecht, R. Steiner, J Derouchey, C. M. Stafford, E. Huang, M Bal, M Tuominen, C. J. Hawker, T. P. Russell, *Adv. Mater.* **2000**, *12*, 787.

[31] S. Park, B. Kim, A. Cirpan, T. P. Russell, *Small* **2009**, *5*, 1343.

[32] B. H. Sohn, B. H. Seo, *Chem. Mater.* **2001**, *13*, 1752.

[33] R. Glass, M. Moller, J. P. Spatz, *Nanotechnology* **2003**, *14*, 1153.

[34] S. I. Yoo, B. H. Sohn, W. C. Zin, S. J. An, G. C. Yi, *Chem. Commun.* **2004**, 2850.

[35] S. I. Yoo, S. J. An, G. Ha. Choi, K. S. Kim, G. C. Yi, W. C. Zin, J. C. Jung, B. H. Sohn, *Adv. Mater.* **2007**, *19*, 1594.

[36] E. Minatti, P. Viville, R. Borsali, M. Shappacher, A. Deffieux, R. Lazzaroni, *Macromolecules* **2003**, *36*, 4125.

[37] M. V. Meli, A. Badia, P. Grutter, R. B. Lennox, *Nano Lett.* **2002**, *2*, 131.

[38] H. Huang, E. E. Remsen, Tomasz Kowalewski, K. L. Wooley, *J. Am. Chem. Soc.* **1999**, *121*, 3805.

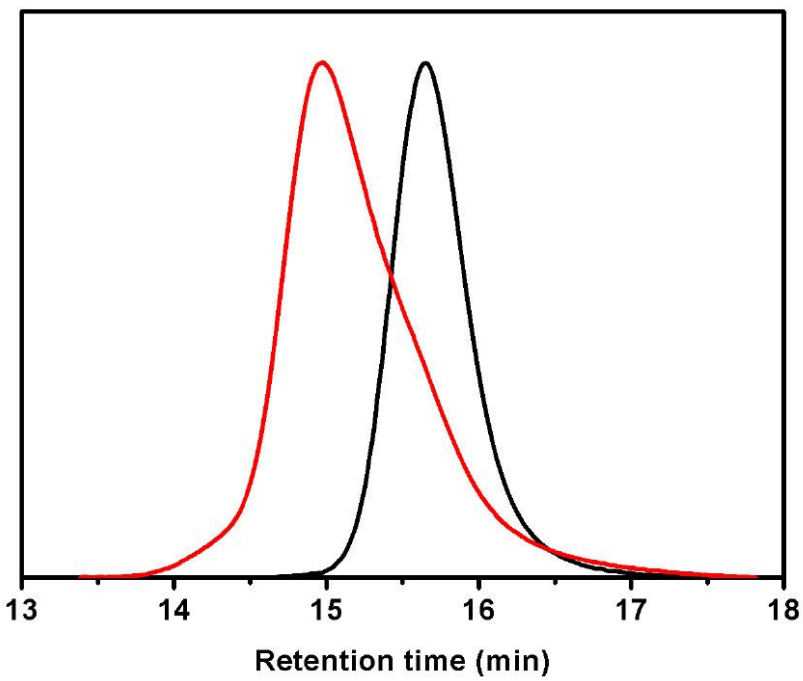

Figure 3.1. GPC profiles for PMMA-macro CTA (black) and PMMA-b-P2VP block copolymers (red).

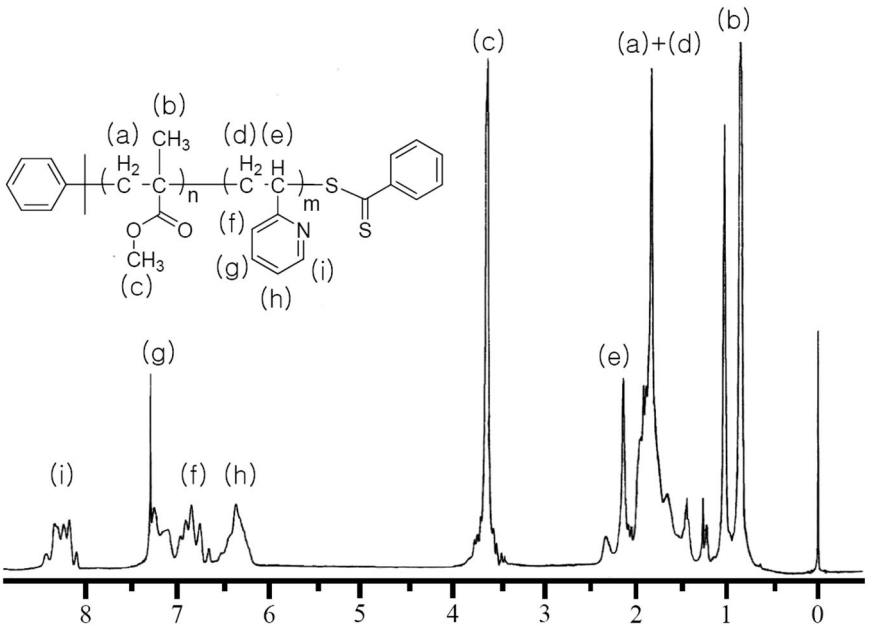

Figure 3.2. ^{1}H NMR spectrum of PMMA-b-P2VP block copolymers. (500 MHz, $CDCl_3$)

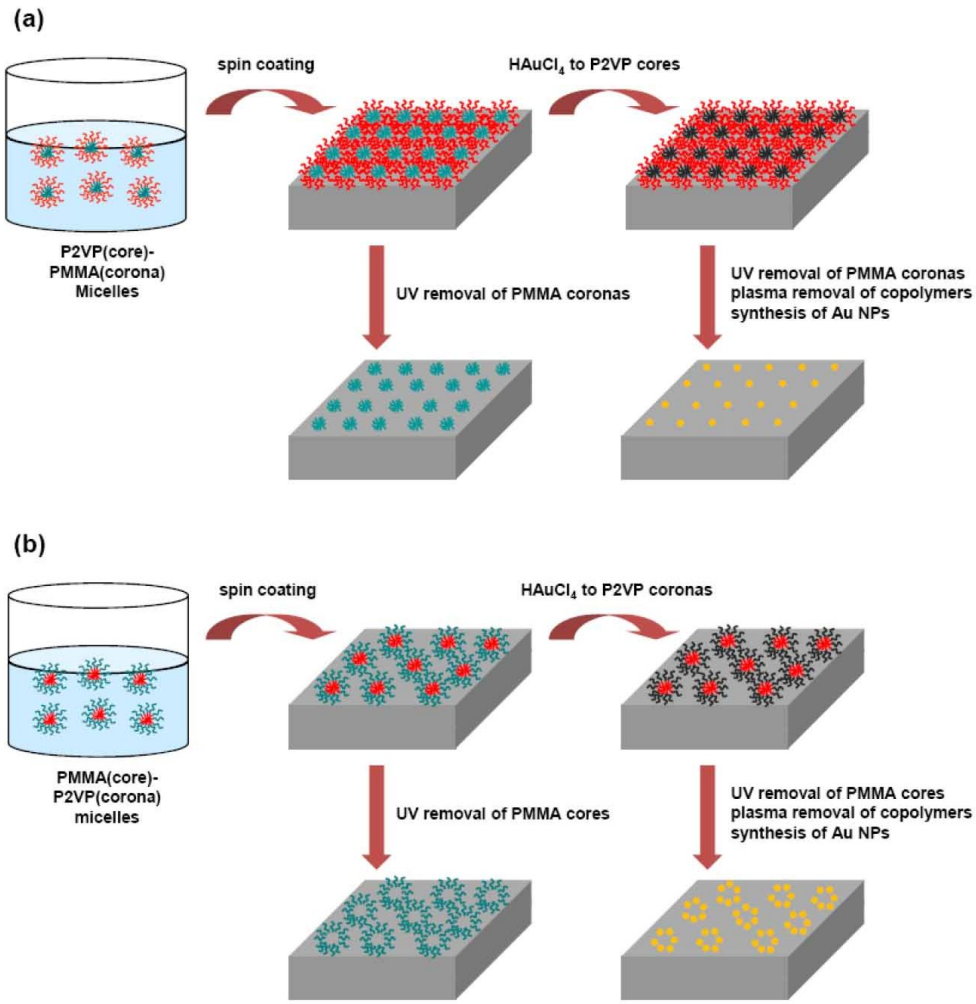

Figure 3.3. Schematic of the fabrication of nanostructures and Au nanoparticles using PMMA-b-P2VP micelles: (a) P2VP(core)-PMMA(corona) micelles; (b) PMMA(core)-P2VP(corona) micelles.

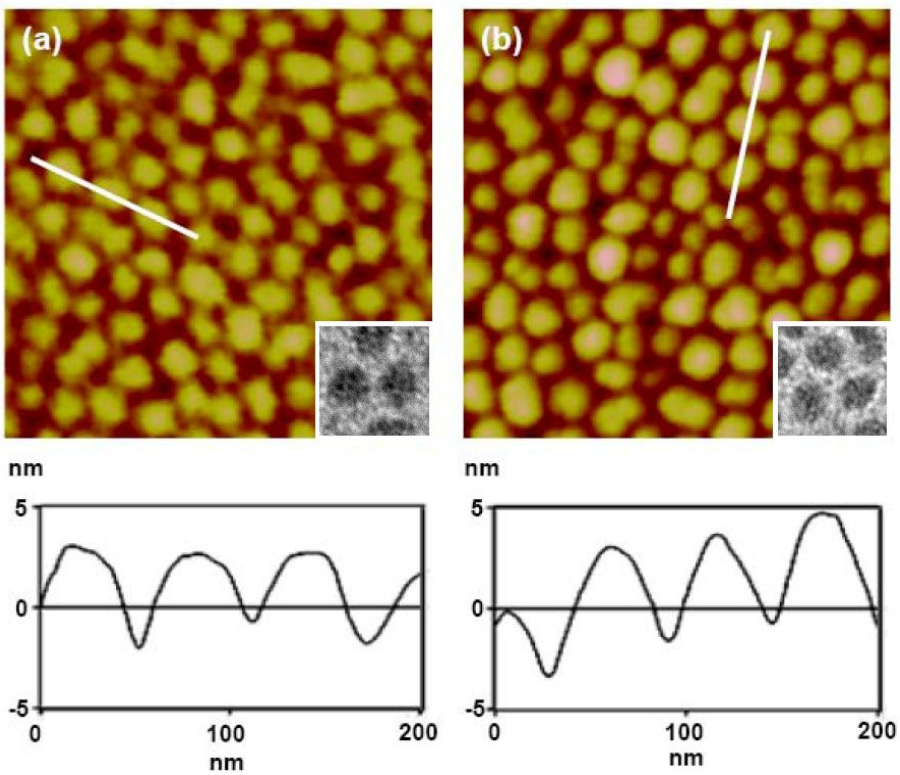

Figure 3.4. AFM images in height mode: (a) P2VP(core)-PMMA(corona) micelles; (b) nanostructures after removal of PMMA coronas. The size of each image is 0.5 μm by 0.5 μm. The height profile along the white line in each image is also displayed. The insets are TEM images (100 nm by 100 nm).

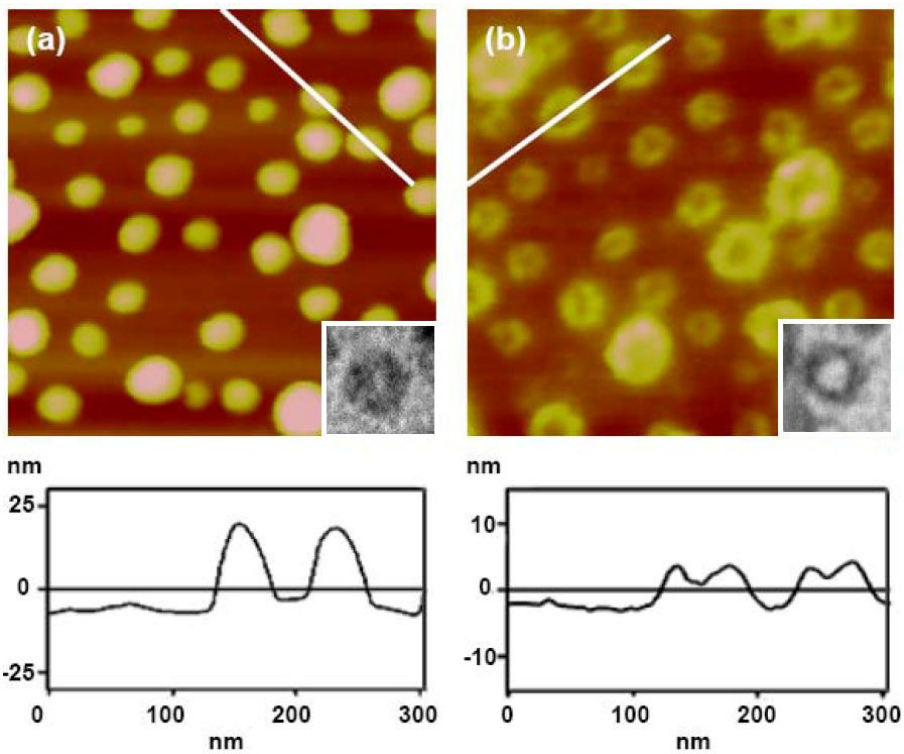

Figure 3.5. AFM images in height mode: (a) PMMA(core)-P2VP(corona) micelles; (b) donut-like nanostructures after removal of PMMA cores. The size of each image is 0.5 μm by 0.5 μm. The height profile along the white line in each image is also displayed. The insets are TEM images (100 nm by 100 nm).

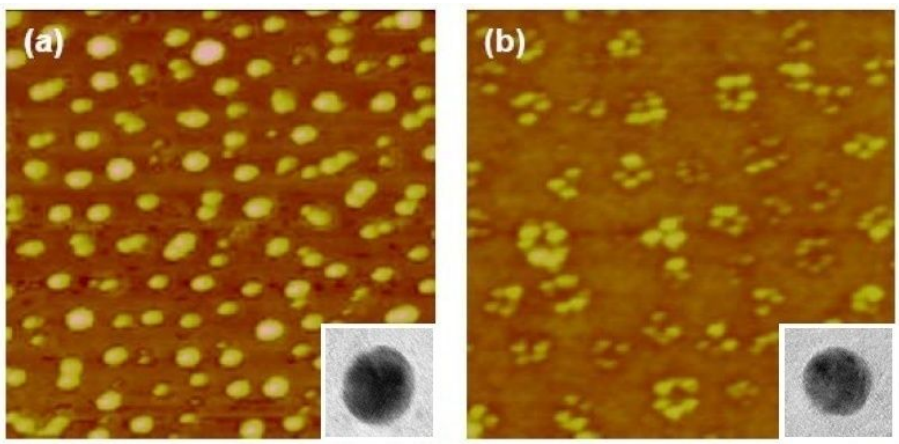

Figure 3.6. AFM images in height mode: (a) gold nanoparticles from P2VP(core)-PMMA(corona) micelles; (b) gold nanoparticles from PMMA(core)-P2VP(corona) micelles. The size of each image is 0.5 μm by 0.5 μm. The insets are TEM images (15 nm by 15 nm).

Chapter 4

Metal Nanoparticle Arrays for Metal-Enhanced Fluorescence in the Framework of Diblock Copolymer Micelles

4.1. Introduction

The conduction electrons in metal nanoparticles (NPs) can be resonantly oscillated by the incident light, which gives rise to a strong electromagnetic field around the surface of NPs.[1-3] Previous studies have been focused on unraveling this phenomenon known as localized surface plasmon resonance on the nearby fluorophores by adjusting several experimental parameters such as the size and shape of NPs, spectral properties of fluorophores, and NP-fluorophore distance.[4-7] From those efforts, it is now understood that metal NPs can concentrate the incident light on the surface of NPs so as to increase the absorption cross-section or the radiative decay rate of nearby fluorophores, which in turn enhances the fluorescence.[8-12] On the other hands, fluorescence can be quenched via non-radiative energy transfer (NET) to metal NPs, particularly when fluorophores are too close to the surface of NPs.[13,14] These features of NP effects are now being implanted in a number of applications necessitating fluorescence signal.[15-20] For example, metal NPs can be inserted into light-emitting diodes to increase the quantum efficiency of the emitting materials.[15] If fluorophore-labeled DNA strands or proteins are bound to metal NPs, the fluorescence can be noticeably enhanced or quenched to allow a sensitive detection of biological reactions.[18]

The solution based synthesis of metal nanoparticles enable to manipulate the size and shape of metal nanoparticles.[21,22] Small spherical metal nanoparticles synthesized by mixture of metal precursor salts and surfactants possess a strong absorption component in their extinction spectrum, potentially quenching the

emission of nearby fluorophores.[23] Seed-mediated synthesis provides metal nanoparticles in diverse shapes with larger dimension [24-26] that tend to enhance fluorescence. These metal nanoparticles can be combined with self-assembling technique such as layer-by-layer assemblies,[27,28] core-shell particles[29,30] and bio-conjugates[31,32] to achieve the spatial arrangement of nanoparticles and fluorophores for the controlled fluorescence. Despite the controlled manner, pre-engaged assemblies require multiple assembling steps to realize tens of nanometers and conformational fluctuation of conjugating flexible materials generates significant deviation in the NP-fluorophore distance. In addition, the transfer of metal nanoparticles or assemblies on a solid substrate for device applications causes random distribution and aggregation of adsorbed metal nanomaterials which can drop the performance of the system over a large area.

These limitations can be overcome by utilization of self-assembling diblock copolymers. In a selective solvent, for example, diblock copolymers self-associate into spherical micelles consisting of soluble coronas and insoluble cores.[33] The diblock copolymer micelles can include precursors of metal nanoparticles in their cores so that ordered arrays of metal nanoparticles can be fabricated by simple coating of micelles and reduction.[34] Since block copolymer micelles produce size-tunable nanodomains in a range of 10 nm to 100 nm depending on the molecular weight of the polymers, the utilization of diblock copolymer micelles enable to control nanostructures of metal nanoparticle in nanoscale. The cores of the micelles can be also further functionalized by fluorophores, such as fluorescent

dyes[35] and quantum dots[36], providing a fixed physical dimension in a thin film state for the effective coupling between photonic nanomaterials, e.g. fluorophores and metal nanoparticles.

In this chapter, we utilize diblock copolymer micelles to organize metal nanoparticle arrays on a solid substrate which can be applied for the plasmon-coupled fluorescence. A single layer of diblock copolymer micelles containing metal precursors in the core blocks was coated on a solid substrate. The nanostructures of micellar arrays of diblock copolymers were transferred to metal nanoparticle arrays by the reduction of metals and the elimination of polymers. The distance between metal nanoparticles was controlled by the intermicellar distance in a single layer of diblock copolymer micelles. These metal nanoparticles arrays were applied as a seed for the growth of larger metal nanoparticles with controlled size and interparticle distance. Diblock copolymer micelles were also employed for the isolation of organic fluorophores in the micellar cores. A thin film of diblock copolymer micelles with organic dyes was combined with metal nanoparticle arrays to verify the strategy of metal-coupled fluorescence enhancement in the hybrid which has fixed distance between dyes and metal nanoparticles determined by micellar nanostructures.

4.2. Experimental Section

PS(109)-P4VP(27) micelles

Diblock copolymers of polystyrene-poly(4-vinylpyridine), PS(109)-P4VP(27) and PS(51)-P4VP(18), were purchased from Polymer Source, Inc. The number in the parenthesis is a number average molecular weight in kg/mol. The polydispersity index (PDI) is 1.12 for PS(109)-P4VP(27) and 1.15 for PS(51)-P4VP(18). Rhodamine 123 (R123) and $HAuCl_4 \cdot 3H_2O$ was purchased from Sigma-Aldrich.

We first dissolved PS(109)-P4VP(27) copolymers in THF, which is compatible to both PS and P4VP blocks in low concentration, to yield a 0.5 wt% solution. Toluene, which is a selective solvent for the PS block, was added dropwise to the THF solution with stirring until the weight ratio of toluene to THF reached to1. Then, THF was completely evaporated at 80 ℃ to obtain a toluene solution of PS(109)-P4VP(27) micelles.

Au nanoparticle arrays

For incorporation of Au nanoparticle precursors into the P4VP core block of PS-P4VP micelles, we stirred the mixture of $HAuCl_4 \cdot 3H_2O$ and PS(109)-P4VP(27) micellar solution without exposure to the light. The molar ratio of $HAuCl_4 \cdot 3H_2O$ to 4VP was equal to 0.2.

The PS(109)-P4VP(27) micellar solution containing $HAuCl_4$ was spin coated (2000 rpm for 1 min) on piranha-washed SiO_2 wafers or quartz. We used 0.1 wt%,

0.15 wt% and 0.2 wt% micellar solution to control the distance between micelles in arrays. Then, O_2 plasma (100 W, 5.0×10^{-2} Torr) was treated for 10 min to reduce Au nanoparticles and to eliminate organic polymers simultaneously.

Ag nanoparticle arrays grown from Au seeds

We synthesized Ag nanoparticle arrays by using Au nanoparticle arrays as seeds, following the modified procedure of the previous report.[39] Growth solution included sodium dihydrogenphosphate (NaH_2PO_4) in DI water with pH 7. After 0.1 mM hydroquinone in DI water and 0.1 mM $AgNO_3$ in DI water with the same volume were sequentially added, a substrate with Au nanoparticle arrays was immersed into the Ag growth solution for 10 min. Then, the substrate was washed with DI water and dried under N_2 flow. Growth by dipping in the Ag growth solution was repeated to obtain larger Ag nanoparticles.

Hybrid of Ag nanoparticle arrays and dye-encapsulated PS-P4VP micelles

We prepared 0.5 wt% PS(51)-PVP(18) micellar solution by directly dissolving copolymer powders in toluene, followed by stirring at 80 ℃ for 6 h and cooling down to room temperature. The organic dye molecule of R123 was added to the micellar solution and the solution was vigorously stirred for ~ 7 day. The molar ratio of R123 to 4VP unit was 0.005.

PS(51)-P4VP(18) micelles with R123 was spin-coated (2000 rpm for 1 min) to fabricate a single layered thin film on substrates with Ag nanoparticle arrays. For

the comparison, a single layer of PS(51)-P4VP(18) micelles was also fabricated on a neat substrate without Ag nanoparticles.

Characterization

UV-Vis absorbance was measured using Varian Cary-5000 spectrophotometer. Steady-state fluorescence was obtained using an Acton SpectraPro with a He-Cd laser (442 nm) as the excitation source. All measurements were performed at room temperature. Transmission electron microscopy (TEM) was performed on a Hitachi 7600 operating at 100 kV. Field-emission scanning electron microscopy (FE-SEM) and atomic force microscopy (AFM) were carried out on a JSM-6700F JEOL and Nanoscope IIIA, Digital Instrument, respectively.

4.3. Results and Discussion

Diblock copolymer of polystyrene-poly(4-vinylpyridine) (PS-P4VP) which consists of a non-polar PS block and a polar P4VP block. PS-P4VP micelles can include metal precursor salts in the P4VP core block such that metal nanoparticles are synthesized in the micelles by reduction.[40] These micelles containing metallic substances are also feasible to produce metal nanoparticle arrays on a solid substrate by simple coating method such as spin coating and dip coating.[41]

We first selected PS(109)-P4VP(27) micelles for the synthesis and arrangement of metal nanoparticles. The number in the parenthesis is a number average molecular weight in kg/mol. In Figure 4.1a, a spherical micelle of the dark P4VP core with the gray PS corona is visible. P4VP cores were selectively stained with I_2 vapor. We obtained the average core diameter of ~21 nm in the TEM image over a larger area and hydrodynamic diameter of ~118 nm by DLS analysis (Figure 4.1b).

To incorporate metal precursors into the P4VP core block of PS(109)-P4VP(27) micelles, $HAuCl_4 \cdot 3H_2O$, a precursor of an Au nanoparticle, was mixed to micellar solution and stirred vigorously without exposure to the light. The molar ratio of $HAuCl_4$ to 4VP was equal to 0.2. $HAuCl_4$ protonates the 4VP in the micellar core, then, $AuCl_4^-$ binds in the core block as a counterion.[41] By spin coating 0.1 wt% PS(109)-P4VP(27) micellar solution containing $HAuCl_4$ in their cores on SiO_2 wafers or quartz which were washed by piranha solution, a single layer of PS(109k)-P4VP(27k) micelle arrays were obtained as shown in Figure 4.2a.

In the AFM image in the height mode, micelles were appeared as bright spheres, clearly showing arrays of micelles on the entire surface of a substrate without aggregation. The average center-to-center distance between micelles was ~118 nm.

Micellar arrays incorporating metal precursors can be transformed to metal nanoparticle arrays by reduction of metal and elimination of organic polymers. After O_2 plasma treatment capable of these two processes simultaneously, Au nanoparticle arrays were obtained (Figure 4.2b). Reduction of the size of spheres ensures polymeric PS-P4VP micelles were totally removed. The average center-to-center distance of Au nanoparticles was ~118 nm, the same to those of micellar arrays, indicating a single layer of micelle arrays guided the spatial arrangement of Au nanoparticles.

The distance between the micelles in arrays, which were fabricated by spin-coating, can be controlled by the concentration of micellar solution. When micellar arrays were fabricated by spin-coating of 0.15 wt% and 0.2 wt% micellar solution containing $HAuCl_4$,the average center-to-center distances between micelles were ~95 nm and ~74 nm, respectively (Figure 4.3ab). Comparison of Figure 4.3 to Figure 4.2 indicates higher concentration of micellar solution induced reduction of the intermicellar distances. By O_2 plasma treatment of micellar arrays in Figure 4.3ab, Au nanoparticle arrays were also generated (Figure 4.3cd). In addition, the distances between Au nanoparticles were unchanged compared to those of original micellar arrays in the both cases. Therefore, we were able to control the structure of metal nanoparticle arrays by manipulation of PS-P4VP micellar arrays in a single

layer.

Metal nanoparticles, e.g. Au and Ag, in arrays on a solid substrate are potentially applicable for the light manipulation of nearby fluorophores.[8] Metal-enhanced fluorescence requires large nanoparticles which have large scattering cross-section directly related to emission enhancement.[8] In the other hand, small nanoparticles induce quenching of fluorescence. For the enhanced intensity of metal-coupled fluorescence, Au nanoparticles which are larger than 40 nm in the diameter are essential.[8] The average diameter of Au nanoparticles in arrays fabricated by PS(109)-P4VP(27) micelles are ~20 nm, expecting quenching of fluorescence would be dominated.

Alternatively, Au nanoparticles can be applied as seeds to synthesize other nanoparticles with large dimension.[39]. We employed Au nanoparticle arrays to grow Ag nanoparticles, which are interactive with fluorescence in visible range,[17] on a substrate. We prepared the Ag growth solution which consists of hydroquinone as a reducing agent and $AgNO_3$ as an Ag precursor. The substrate of Au nanoparticle arrays were immersed into the Ag growth solution for 10 min and thoroughly washed with DI water followed by drying under N_2 flow. We repeated the growth step to control the size of Ag nanoparticles with larger diameter.

AFM images in Figure 4.4a-c show Ag nanoparticle arrays grown from Au nanoparticle arrays on a substrate. Ag nanoparticles were evenly distributed on entire substrate without significant aggregation. As the growth steps were repeated, the diameter of Ag nanoparticles gradually increased (45 nm by 1 cycle, 58 nm by

3 cycles, 70 nm by 5 cycles). Growth of Ag nanoparticles was also proved that the peak of UV-Vis absorbance is red-shift from 364 nm for Ag with 45nm diameter to 419 nm for Ag with the diameter of 70 nm (Figure 4.4d). It is assumed that irregular shapes of Ag nanoparticles result from the different growth rate depending on crystalline facets.[42]

Regardless of the growth cycle, the average center-to-center distance of Ag nanoparticles were ~118 nm which is the same value to those of micellar arrays and Au nanoparticle arrays. The constant interdistance of micellar arrays, Au nanoparticle arrays and Ag nanoparticle arrays supports that the arrangement of metal nanoparticles can be guided by micellar arrays on a substrate. Since the interdistance between micelles or Au nanoparticles is controlled by the concentration of micellar solution, we synthesize Ag nanoparticle arrays with different interparticle distance by using Au nanoparticle arrays fabricated from spin-coated a 0.2 wt% micellar solution in Figure 4.3c. With the same Ag growth condition, Ag nanoparticle arrays with controlled sizes were fabricated on a substrate (Figure 4.5a-c). By the growth for 1 cycle, 3 cycles and 5 cycles, Ag nanoparticle were synthesized with diameters of ~36 nm, ~58 nm and ~64 nm respectively, supported by red-shifted peak of absorbance from 382 nm to 412 nm as the size of Ag nanoparticles increased (Figure 4.5d). From AFM images of Figure 4.5, the average center-to-center distance of Ag nanoparticles was ~74 nm which is the same distance of arrays of micelles in Figure 4.3b and Au nanoparticles in Figure 4.3d. Therefore, the nanostructures of Ag nanoparticle

arrays were precisely controlled by arranged micellar arrays and the growth cycles to determine the interparticle distance and the size of nanoparticles respectively. We note that the red shift of absorbance peak by the plasmonic coupling between Ag nanoparticles can be ignored because of very weak coupling or decoupling between Ag nanoparticles separated by more than 10 nm.[45]

We applied Ag nanoparticle arrays as a substrate for the control of fluorescence.[8] For fluorescence enhancement by coupling with metal nanoparticles, we consider the distance between fluorophores and the surface of a metal nanoparticle because close contact of two components results in quenching of fluorescence by near surface energy transfer from a excited fluorophore to a metal nanoparticle.[8] Self-assembled micelles of block copolymers enable to effectively alienate fluorophores from the coupled metal nanoparticles in a thin film.[43]

For this purpose, we selected a single layer of PS(51)-P4VP(18) micelles encapsulating R123, a green emitting organic dye, in the P4VP cores. PS(51)-P4VP(18) formed micelles in toluene as PS(109)-P4VP(27) did. R123 with the molar ratio of 0.005 to 4VP was incorporated in a 0.5 wt% PS(51)-P4VP(18) micellar solution with vigorous stirring for 7 days. In the TEM image of Figure 4.6a, PS(51)-P4VP(18) the dark P4VP cores, stained by I_2 vapor, are discernible in a single-layered thin film. The average core diameter was ~27 nm and the center-to-center distance between micelles was ~53 nm. The absorbance and emission peak of R123 encapsulated in PS(51)-P4VP(18) micelles were 525 nm and 548 nm

respectively (Figure 4.6b).

PS(51)-P4VP(18) micelles with R123 was spin coated on substrates of Ag nanoparticle arrays which have the center-to-center distance between Ag nanoparticles was 118 nm in Figure 4.4so that hybrid of metal nanoparticles and micelles with R123 was obtained (Figure 4.7a-c). We also prepared a thin film of PS(51)-P4VP(18) micelles with R123 on a neat substrate as a reference. AFM images with corresponding FE-SEM images clearly show arrays of spherical micelles with bright Ag nanoparticle arrays. Micelles were not covered Ag nanoparticles but coated on the unoccupied areas between Ag nanoparticles. In the color-modified AFM image of Ag nanoparticles with the diameter of 70 nm, about six small micelles surrounded single Ag nanoparticle and each micelle closely contacted to Ag (Figure 4.8). We note that a few micelles are located on a large Ag nanoparticle in Figure 4.7c, but their population can be ignored compared to that of micelles in arrays.

In these hybrid, fluorescence of R123 in the core block of PS(51)-P4VP(18) micelles can be affected nearby Ag nanoparticles. Figure 4.9a is PL spectra of miellar arrays with R123 on a neat substrate and on Ag nanoparticle arrays. Emission intensities of R123 were reduced by 22% on Ag nanoparticles with the diameter of 45 nm and increased 1.78 and 2.65 times on Ag nanoparticle arrays with the diameter of 58 nm and 70 nm, respectively. For the quantitative analysis, we considered that the number of micelles on Ag nanoparticle arrays is less than that on a neat substrate. We calculated 87 %, 79 % and 72 % of unoccupied area of

Ag nanoparticle substrates. Enhancement factors of R123 emission were recalculated to 0.90, 2.25 and 3.68 on Ag nanoparticles with the diameter of 45 nm, 58 nm and 70 nm respectively. Therefore, fluorescence of R123 in the core block of micelles was effectively changed on Ag nanoparticles arrays.

Enhancement of fluorescence by metal nanoparticles is affected by the distance between fluorophores and the surface of metal nanoparticles[8] and spectral overlap among absorbance of metal nanoparticles, excitation wavelength and absorbance and emission of fluorophores.[32] R123 encapsulated into the core of PS(51)-P4VP(18) micelles is apart from the Ag nanoparticles by 13~40 nm, analyzed by the TEM image in Figure 4.6, which is effective for fluorescence enhancement with the restriction of both non-radiative energy transfer from dyes to metal nanoparticles by close contact and decoupling of dye-NP by the far separation.[8] In the aspect of the spectral overlap, absorbance of Ag nanoparticles is matched with excitation wavelength, resulting in enhancement of excitation intensity. Moreover, in hybrid of Ag nanoparticles and PS-P4VP micelles, absorbance of Ag nanoparticles broadly covered visible wavelength so that spectral overlap between Ag nanoparticles and R123 was effective, enabling fluorescence enhancement by increasing radiative decay rate. Since larger Ag nanoparticles show effective spectral overlap with R123, enhancement factor of R123 emission was presumably larger on Ag nanoparticles with the size of 70 nm than on the Ag nanoparticles with the diameter of 58 nm. On the other hand, slight quenching of R123 emission on the Ag with the diameter of 45 nm is presumably explained that

the spectral overlay between R123 and Ag nanoparticles was insufficient and the absorption scattering cross-section of small Ag nanoparticles were comparable to restrict the enhancement of fluorescence.[8] The analysis of time-resolved photoluminescence would provide the quantitative characterization of enhancement factors of excitation and radiative decay rate.[44]

4.4. Conclusions

Emission of fluorescence can be manipulated by coupling with localized surface plasmon of nearby metal nanoparticles. For metal-enhanced fluorescence, the control of the size of nanoparticles and the distance between fluorophores and nanoparticles is inevitable. We utilized diblock copolymer micelles as a template to arrange metal nanoparticles on a solid substrate. The nanostructures of metal nanoparticle arrays were precisely managed by micellar arrays of diblock copolymers. We also controlled the size of metal nanoparticles by chemical growth approach. Diblock copolymer micelles were also successfully employed for organization of fluorophores with metal nanoparticle array to achieve metal enhanced fluorescence. The demonstration here can extend to applications for arrangement of a variety of nanoparticles in controlled manner by utilization of diblock copolymer micelles. In addition, diblock copolymer micelles can provide the effective coupling between fluorophores and metal nanoparticles by controlling the distance, applicable to light emitting devices with high performances.

4.5. References

[1] E. Hutter, J. H. Fendler, *Adv. Mater.* **2004**, *16*, 1685.

[2] A. Moores, F. Goettmann, *New J. Chem.* **2006**, *30*, 1121.

[3] D. M. Solís, J. M. Taboada, F. Obelleiro, L. M. Liz-Marzán, F. J. G. de Abajo, *ACS Nano* **2014**, *8*, 7559

[4] V. Giannini, A. I. Fernández-Domínguez, S. C. Heck. S. A. Maier, *Chem. Rev.* **2011**, *111*, 3888.

[5] T. Ming, H. Chen, R. Jiang, Q. Li, J. wang, *J. Phys. Chem. Lett.* **2012**, *3*, 191.

[6] A. M. Kern, D. Zhang, M. Brecht, A. I. Chizhik, A. V. Failla, F. Wackenhut, A. J. Meixner, *Chem. Soc. Rev.* **2014**, *43*, 1263.

[7] K. G. Stamplecoskie, J. C. Scaiano, *J. Phys. Chem. C* **2011**, *115*, 1403.

[8] J. R. Lakowicz, *Anal. Biochem.* **2005**, *337*, 171.

[9] S. Khatua, M. Orrit, *J. Phys. Chem. Lett.* **2014**, *5*, 3000.

[10] M. Bauch, K. Toma, M. Toma, Q, Zhang, J. Dostalek, *Plasmonics* **2014**, *9*, 781.

[11] R. Bardhan, N. K. Grady, J. R. Cole, A. Joshi, N. J. Halas, *ACS Nano* **2009**, *3*, 744.

[12] P. P. Pompa, L. Martiradonna, A. Della Torre, F. Della Sala, L. Manna, M. De Vittorio, F. Calabi, R. Cingolani, R. Rinaldi, *Nat. Nanotechnol.* **2006**, *1*, 126.

[13] C. S. Yun, A. Javier, T. Jennings, M. Fisher, S. Hira, S. Peterson, B. Hopkins, N. O. Reich, G. F. Strouse, *J. Am. Chem. Soc.* **2005**, *127*, 3115.

[14] X. Zhang, C. A. Marocico, M. Lunz, V. A. Gerard, Y. K. Gun'ko, V. Lesnyak,

N. Gaponik, A. S. Susha, A. L. Rogach, A. L. Bradley, *ACS Nano* **2012**, *6*, 9283.

[15] L. W. Jang, D. W. Jeon, M. Kim, J. W. Jeon, A. Y. Polyakov, J. W. Ju, S. J. Lee, J. H. Baek, J. K. Yang, I. H. Lee, *Adv. Funct. Mater.* **2012**, *22*, 2728.

[16] F. Liu, J. M. Nunzi, *Org. electronics* **2012**, *13*, 1623.

[17] W. Deng, E. M. Goldys, *Langmuir* **2012**, *28*, 10152.

[18] R. Schreiber, J. do, E. M. Roller, T. Zhang, V. J. Schüller, P. C. nickels, J. Feldmann, T. Liedl, *Nat. Nanotechnol.* **2014**, *9*, 74.

[19] J. M. Liu, J. T. Chen, X. P. Yan, *Anal. Chem.* **2013**, *85*, 3238.

[20] Z. Jiang, B. Dong, B. Chen, J. Wang, L. Xu, S. Zhang, H. Song, *Small* **2013**, *9*, 604.

[21] M. Rycenga, C. M. Cobley, J. Zeng, W. Li, C. H. Moran, Q. Zhang, D. Qin, Y. Xia, *Chem. Rev.* **2011**, *111*, 3669.

[22] M. Grzelczak, J. Pérez-Juste, P. Mulvaney, L. M. Liz-Marzán, *Chem. Soc. Rev.* **2008**, *37*, 1783.

[23] E. Dulkeith, M. Ringler, T. A. Klar, J. Feldmann, *NanoLett.* **2005**, *5*, 585.

[24] Y. J. Lee, N. B. Schade, L. Sun, J. A. Fan, D. R. Bae, M. M. Mariscal, G. Lee, F. Capasso, S. Sacanna, V. N. Manoharan, G. R. Yi, *ACS Nano* **2013**, *7*, 11064.

[25] X. Ye, C. Zheng, J. Chen, Y. Gao, C. B. Murray, *NanoLett.* **2013**, *13*, 765.

[26] J. R. Vutukuri, A. Imhof, A. van Blaaderen, *Angew. Chem. Int. Ed.* **2014**, *53*, 13830.

[27] Y. Jin, X. Gao, *Nat. Nanotechnol.* **2009**, *4*, 571.

[28] G. Schneider, G. Decher, N. Nerambourg, R. Praho, M. H. V. Werts, M.

Blanchard-Desce, *NanoLett.* **2006**, *6*, 530.

[29] N. Liu, B. S. Prall, V. I. Klimov, *J. Am. Chem. Soc.* **2006**, *128*, 15362.

[30] M. Lessard-Viger, M. Rioux, L. Rainville, D. Boudreau, *NanoLett.* **2009**, *9*, 3066.

[31] J. Lee, T. Javed, T. Skeini, A. O. Govorov, G. W. Bryant, N. A. Kotov, *Angew. Chem., Int. Ed.* **2006**, *45*, 4819.

[32] Y. Chem, K. Munechika, D. S. Ginger, *NanoLett.* **2007**, *7*, 690.

[33]S. Förster, M. Antonietti, *Adv. Mater.* **1998**, *10*, 195.

[34] S. H. Yun, S. I. Yoo, J. C. Jung, W. C. Zin, B. H. Sohn, *Chem. Mater.* **2006**, *18*, 5646.

[35] S. I. Yoo, S. J. An, G. H. Choi, K. S. Kim, G.-C.Yi, W.-C.Zin, J. C. Jung and B. H. Sohn, *Adv. Mater.* **2007**, *19*, 1594.

[36] M. Moffitt and A. Eisenberg, *Chem. Mater.* **1995**, *7*, 1178.

[37] S. I. Yoo, J. H. Lee, B. H. Sohn, I. Eom, T. Joo, S. J. An, G. C. Yi, *Adv. Funct. Mater.* **2008**, *18*, 2984.

[38] S. I. Yoo, S. H. Bae, K. S. Kim, B. H. Sohn, *Soft Matter* **2009**, *5*, 2990.

[39] A. Sánchez-Iglesias, P. Aldeanueva-Potel, W. Ni, J. Pérez-Juste, I. Pastoriza-Santos, R. A. Alvarez-Puebla, B. N. Mbenkum, L. M. Liz-Marzán, *Nano Today* **2010**, *5*, 21.

[40] G. Rainò, T. Stöferle, C. Park. H. C. Kim, T. Topuria, P. M. Rice, I. J. Chin, R. D. Miller, R. F.Mahrt, *ACS Nano* **2011**, *5*, 3536.

[41] R. Glass, M. Möller, J. P. Spatz, *Nanotechnology* **2003**, *14*, 1153.

[42] Y. Xiang, X. Wu, D. Liu, Z. Li, W. Chu. L. Feng, K. Zhang, W. Zhou, S. Xie, *Langmuir* **2008**, *24*, 3465.

[43] K. S. Kim, H. Kim, J. H. Kim, J. H. Kim, C. L. Lee, F. Laquai, S. I. Yoo, B. H. Sohn, *J. Mater. Chem.* **2012**, *22*, 24727.

[44] K. S. Kim, J. H.. Kim, H. Kim, F. Laquai, E. Arifin, J. K. Lee, S. I. Yoo, B. H. Sohn, *ACS Nano* **2012**, 6, 5051.

[45] C. Tabor, R. Murali, M. Mahmoud. M. A. El-Sayed, *J. Phys. Chem. A* **2009**, *113*, 1946.

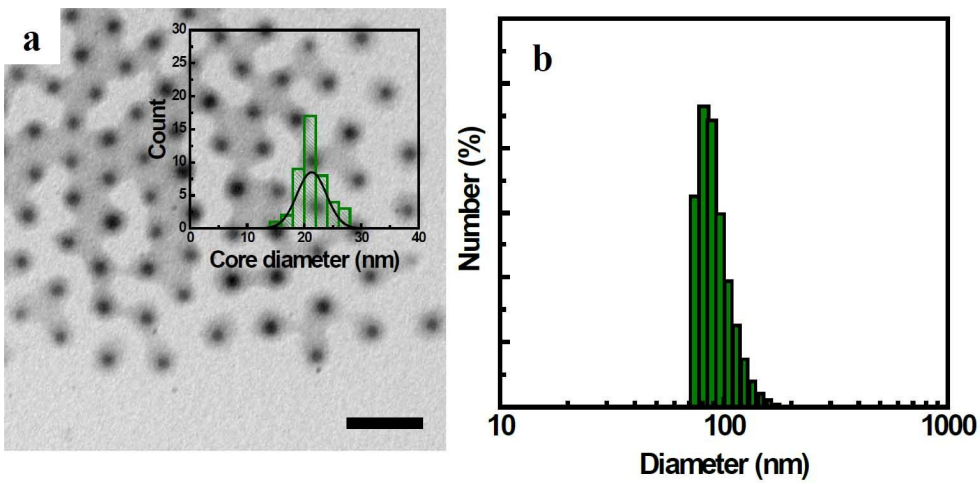

Figure 4.1. (a) TEM image of PS(109)-P4VP(27) micelles; (b) hydrodynamic diameters of PS(109)-P4VP(27) micelles. The Inset in (a) is the distribution of the core diameter of micelles. The scale bar is 100 nm.

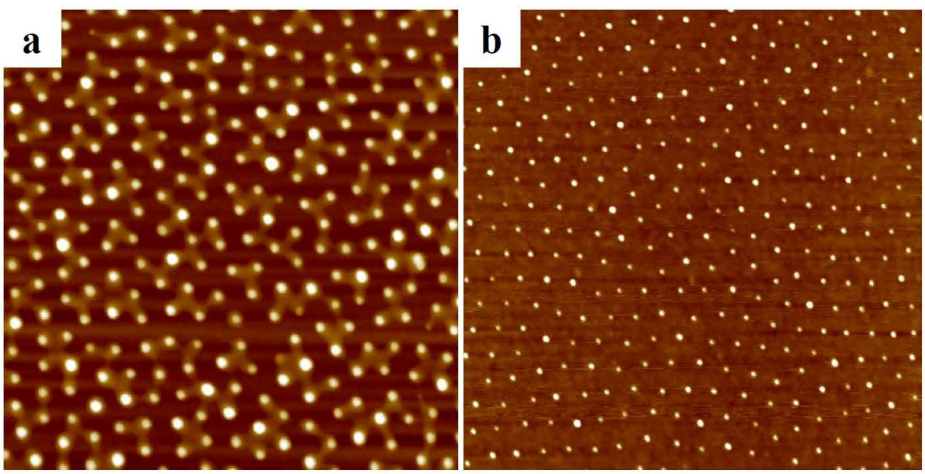

Figure 4.2. AFM images; (a) arrays of PS(109)-P4VP(27) micelles; (b) Au nanoparticle arrays. The size of AFM images is 2 μm by 2 μm.

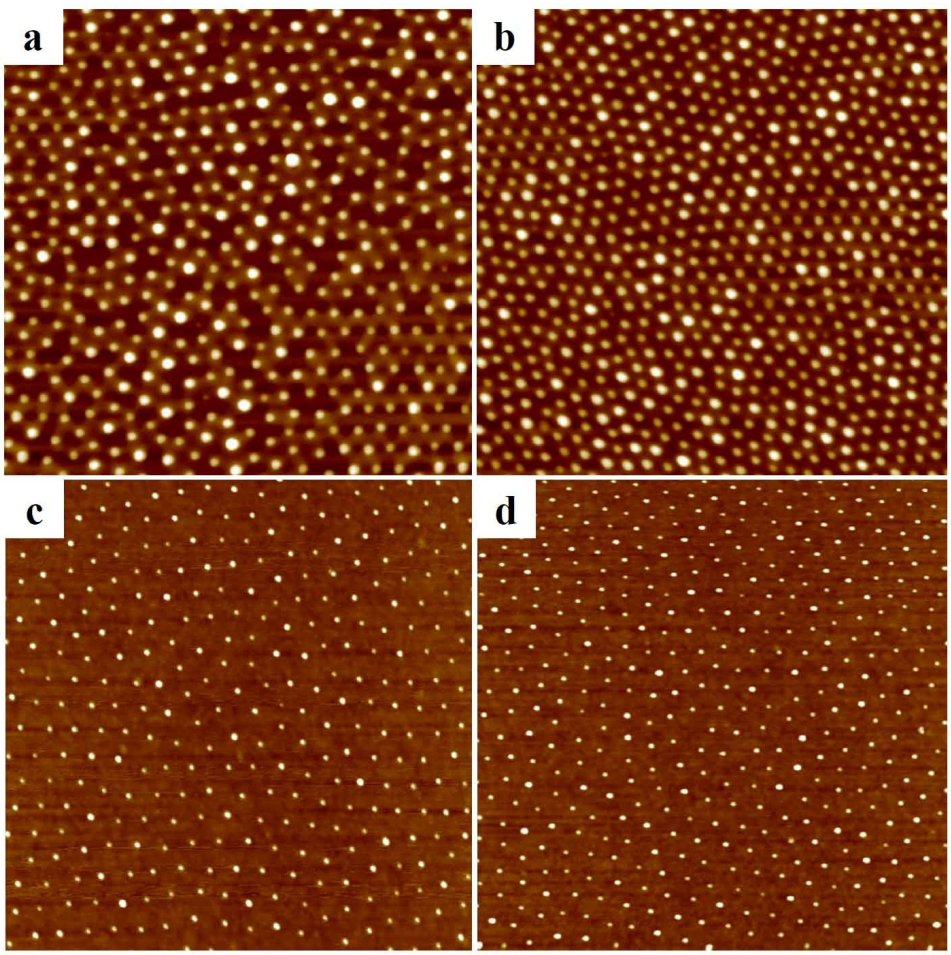

Figure 4.3. AFM images; (a,b) arrays of PS(109)-P4VP(27) micelles from (a) 0.15 wt% and (b) 0.2 wt% micellar solution; (c,d) Au nanoparticle arrays obtained from (a) and (d) respectively. The size of AFM images is 2 μm by 2 μm.

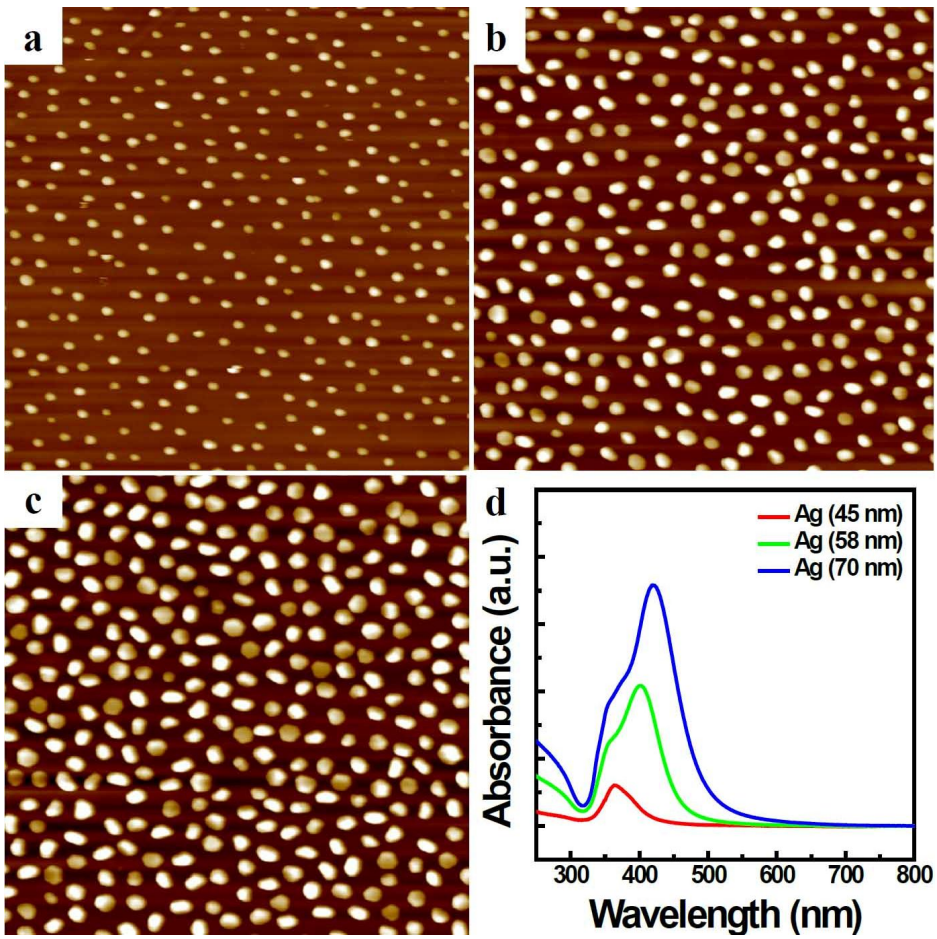

Figure 4.4. (a-c) AFM images of arrays of Ag nanoparticles (the center-to-center distance = 118 nm); Diameters of Ag nanoparticles are (a) 45 nm, (b) 58 nm and (c) 70 nm; (d) UV-Vis spectra of Ag nanoparticle arrays. The size of AFM images is 2 μm by 2 μm.

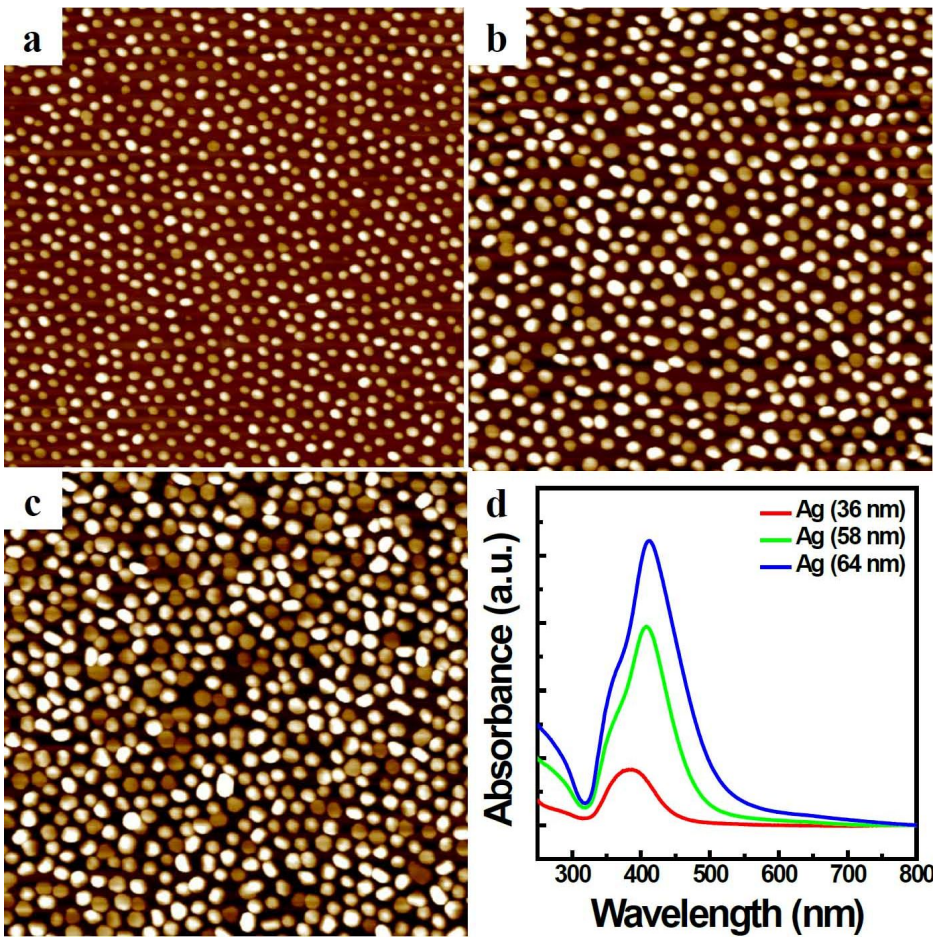

Figure 4.5. (a-c) AFM images of arrays of Ag nanoparticles (the center-to-center distance = 74 nm); Diameters of Ag nanoparticle are (a) 36 nm, (b) 58 nm and (c) 64 nm; (d) UV-Vis spectra of Ag nanoparticle arrays. The size of AFM images is 2 μm by 2 μm.

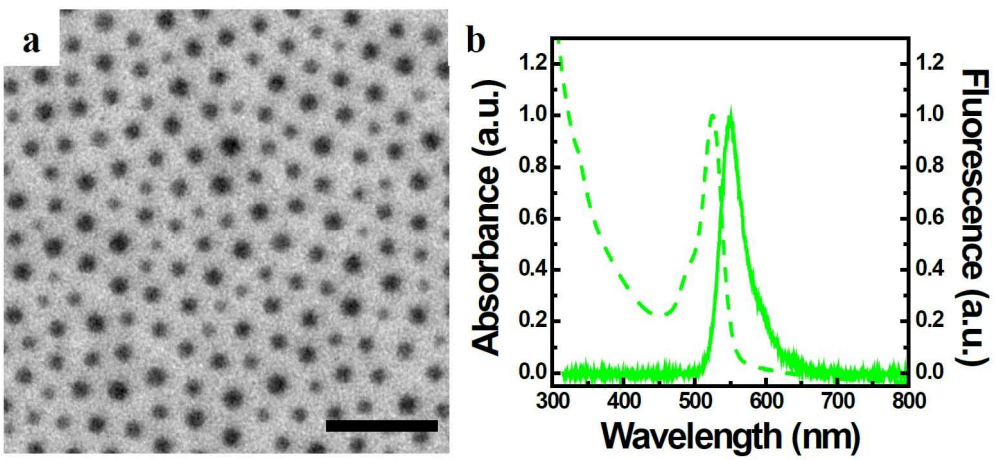

Figure 4.6. (a) TEM image of a single layer of PS(51)-P4VP(18); (b) UV-Vis (dashed) and PL (solid) spectra of R123 encapsulated in PS(51)-P4VP(18) micelles. The scale bar is 100 nm.

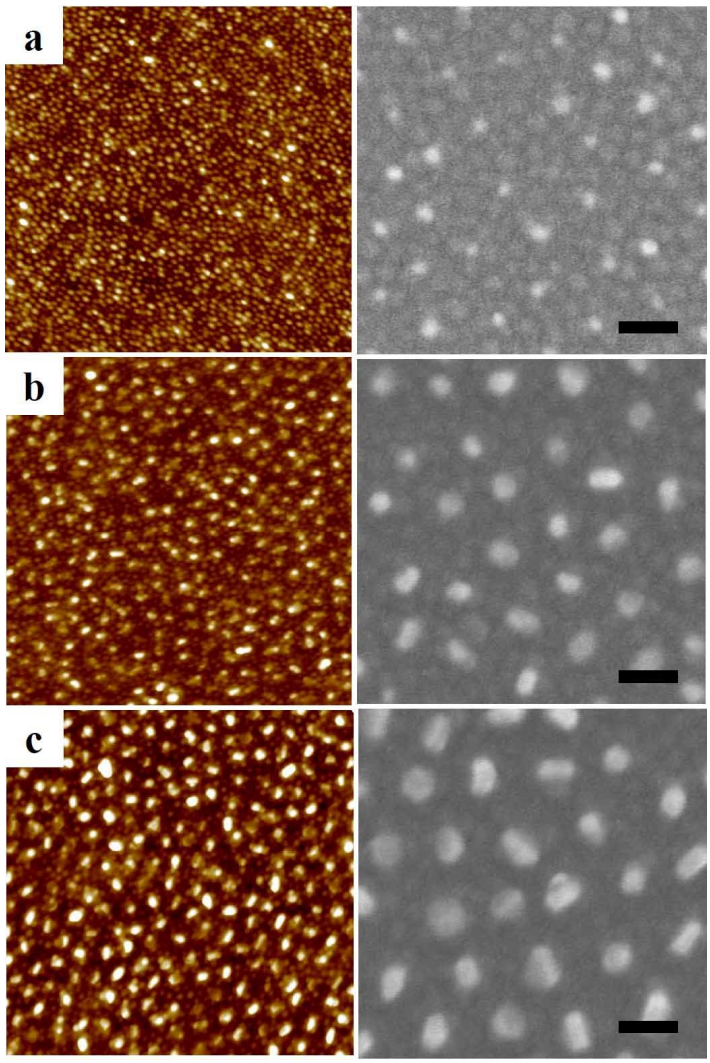

Figure 4.7. AFM images (left column) and corresponding FE-SEM images (right column) of PS(51)-P4VP(18) micellar films on Ag nanoparticle arrays (the center-to-center distance = 118 nm). Diameters of Ag nanoparticles are (a) 45 nm, (b) 58 nm and (c) 70 nm. The size of AFM images is 2 μm by 2 μm. All scale bars in FE-SEM images are 100 nm.

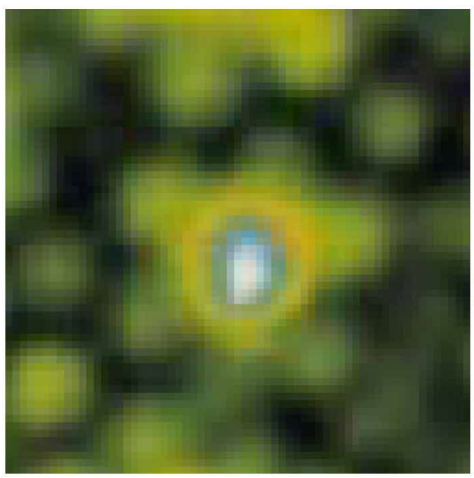

Figure 4.8. Magnified AFM image of Figure 4.7c displayed with modified color profile.

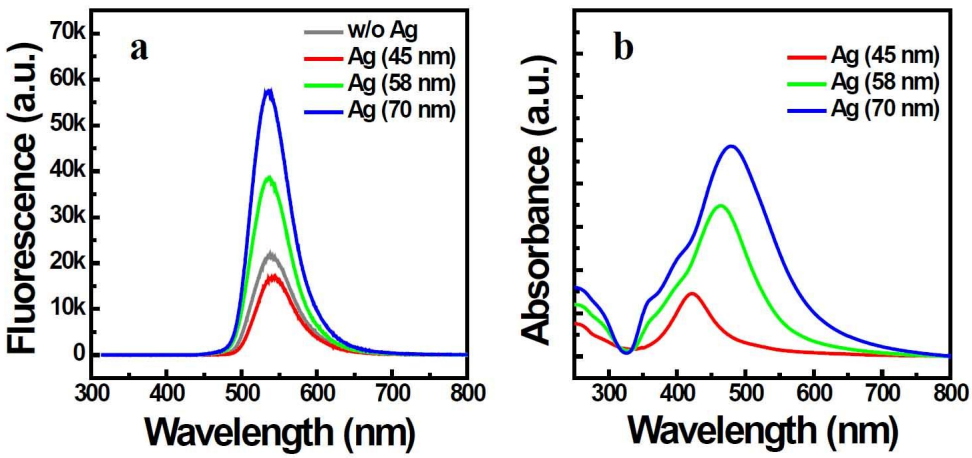

Figure 4.9. (a) PL spectra of R123 in PS(51)-P4VP(18) micelles on Ag nanoparticle arrays; (b) UV-Vis spectra of Ag nanoparticles with PS(51)-P4VP(18) micelles.

Abstract in Korean

블록공중합체 마이셀을 이용한 콜로이드 나노소재 조립 및 배열 제어

김 정 희
화학부 고분자전공
서울대학교 대학원

크기, 모양, 화학적 특성에 따라 독특한 광학적, 전자적, 자극감응 등의 특성을 가질 수 있는 나노미터 크기의 유기, 무기 콜로이드 나노입자는 나노기술 분야의 핵심요소로 도입되어 왔다. 최근에는 단일 콜로이드 나노입자 수준에서의 합성 및 응용에 대한 연구를 기반으로, 시스템 내에서 콜로이드 나노입자의 조합과 공간적 분포를 제어하여 독특한 형태의 나노 또는 마이크로 구조를 구현하고 기능성 콜로이드 나노입자의 응용가능성을 확장하려는 연구가 주목받고 있다.

콜로이드로 구성된 구조의 조절은 콜로이드 간 결합에 의한 조립 제어와 규칙적 구조를 가지는 콜로이드 배열 제어를 포함한다. 콜로이드 나노입자를 단량체로 이용하여 콜로이드 나노입자 사이의 상호작용을

조절하면 콜로이드 간 자기조립에 의한 고차구조가 형성된다. 이러한 콜로이드 조립을 제어하면 자연모방의 계층구조 또는 광학적 특성을 가지는 규칙적인 구조의 구현이 가능하다. 고체 기판 위에서의 콜로이드 나노입자 배열 제어는 콜로이드 나노입자의 디바이스 응용을 위해 중요하다. 광학적, 전자적 기능성을 가지는 콜로이드의 특성은 인접한 콜로이드 간 커플링에 의해 변화할 수 있기 때문에 기판에 분산된 콜로이드의 거리와 배열제어가 필수적이다. 또한 나노스케일 크기의 구조 특성을 가지는 콜로이드 배열은 다른 소재의 나노구조 제조를 위한 나노마스크 또는 나노템플릿으로 활용 가능하다.

콜로이드로 구성된 구조를 구현하기 위해 금속 나노입자와 고분자 콜로이드와 같은 다양한 나노입자가 도입되고 있다. 서로 다른 두 고분자 사슬로 이루어진 블록공중합체는 한쪽 블록에 선택적 용매에서 나노미터 크기의 마이셀로 자기조립 되는데, 이러한 블록공중합체 마이셀을 일종의 고분자 콜로이드 나노입자로 활용할 수 있다. 또한 블록공중합체 마이셀을 나노크기의 콜로이드 템플릿으로 활용하여 다른 소재의 콜로이드 나노구조의 제조에 활용할 수 있다.

본 연구에서는 이중블록공중합체 마이셀을 이용하여 콜로이드 조립구조를 구현하고 콜로이드 나노입자의 배열을 제어하였다. 이중블록공중합체 마이셀을 콜로이드 단위블록으로 활용하여 용액상에서 형태가 제어된 콜로이드 조립구조 구현이 가능하였다. 또한

이중록공중합체 마이셀을 템플릿으로 활용하여 고체기판 위에서 금속 나노입자 배열을 합성 및 조절하였다. 이렇게 제조된 금속 나노입자 배열은 형광체를 포함한 이중블록공중합체와 조합하여 금속과 형광체의 커플링에 의한 형광특성을 조절할 수 있는 기판으로 활용하였다.

제1장에서는 이중블록공중합체의 마이셀 형성에 대해 개괄하였다. 이중블록공중합체가 한쪽 블록에 선택적인 용매에 분산되면 미세상 분리에 의해 용해되는 코로나 블록과 용해되는 않는 코어 블록으로 이루어진 구형 마이셀로 자기조립된다. 마이셀의 나노구조는 블록공중합체의 분자량과 블록의 구성비에 의해 정밀하게 제어 가능하다. 이러한 이중블록공중합체 마이셀은 나노크기의 고분자 콜로이드로 응용이 가능하다. 또한 마이셀의 코어블록에 유기형광체나 금속전구체와 같은 기능성 물질의 선택적 도입이 가능하여 유기 또는 무기 콜로이드 나노소재의 정렬된 배열을 구현하기 위한 템플릿으로 활용이 가능하다.

제 2장에서는 이중블록공중합체 마이셀이 조립된 콜로이드 고분자를 보고하였다. 극성 블록과 비극성 블록으로 구성된 이중블록공중합체를 이용하여 비극성 용매에서 구형 마이셀을 제조하였다. 극성의 코어 블록을 가교한 후 코어 블록과 코로나 블록이 모두 용해되도록 용매환경을 변화시켰다. 가교된 코어 블록은 완벽하게 용해되지 않지만 코로나 사슬을 재배열하여 용매에 노출된다. 이로 인해 구형의 마이셀은 용매에 노출된 극성 코어 블록을 중심으로 양쪽에 비극성 코로나 블록이

위치한 독특한 콜로이드 구조를 형성한다. 이러한 콜로이드 구조를 단량체로 활용하여 용매의 극성을 증가시켜 마이셀 콜로이드가 중합된 콜로이드 고분자 사슬을 구현하였다. 동일한 과정을 통해 분자량이 큰 마이셀과 분자량이 작은 마이셀로부터 콜로이드 고분자사슬을 제조하였으며 이들의 조합을 조절하여 랜덤 또는 블록 형태의 콜로이드 중합체 사슬을 구현하였다.

제 3장에서는 나노입자의 합성이 가능한 블록과 선택적 제거가 가능한 블록으로 구성된 블록공중합체를 RAFT 중합법으로 합성하였다. 각 블록에 대한 선택적 용매를 사용하여 나노입자 합성이 가능한 코어블록과 선택적 제거가 가능한 코로나 블록 또는 두 블록이 반대로 위치한 두 종류의 구형 마이셀을 제조하였다. 이러한 마이셀을 기판 위에 코팅하여 마이셀 단일층을 제조하였다. 제조된 마이셀 나노구조를 금 나노입자의 배열을 제어하는 템플릿으로 활용하여 대면적에 균일하게 분산된 금 나노입자와 고리 형태로 정렬된 금 나노입자 배열을 구현하였다.

제 4장에서는 단일층의 이중블록공중합체 마이셀을 이용하여 금속 나노입자 배열의 구조를 제어하였다. 우선 코어 블록에 금속 전구체가 선택적으로 도입된 단일층의 마이셀을 기판 위에 코팅하였다. 금속 나노입자를 환원하고 고분자를 제거하여 마이셀 배열의 구조가 전사된 금속 나노입자 배열을 구현하였다. 배열되는 금속나노 입자 간 거리는

마이셀 배열의 간격을 제어하여 조절이 가능하였다. 이렇게 제조된 나노입자 배열로부터 금속 나노입자를 성장시켜 크기와 간격이 조절된 금속 나노입자 배열을 제조하였다. 제조된 금속 나노입자 배열과 형광체가 도입된 이중블록공중합체를 조합하여 금속 나노입자와 형광체의 커플링에 의한 형광 제어를 확인하였다.

주요어: 콜로이드 나노입자, 콜로이드 조립, 이중블록공중합체, 마이셀, 자기조립, 콜로이드 고분자, 금속 나노입자, 형광

학 번: 2008-20313

Curriculum Vitae

Name: Jeong-Hee Kim

Date of Birth: October 10, 1982.

Educations

2008.03 ~ 2015.02 Seoul National University, Ph. D degree in the Department of Chemistry (Polymer Chemistry)
Thesis: Controlled Organization of Colloidal Nanomaterials with Block Copolymer Micelles

2001.03 ~ 2008.02 Seoul National University, Bachelor's degree in the Department of Chemistry

Areas of Research Interests

Self-assembled nanostructures and superstructures of block copolymers

Nanopatterns of metal and inorganic materials

Photonic coupling of fluorescence and plasmon in nanostructured thin films

Publications

<International>

[1] **Jeong-Hee Kim**, Won Jong Kwon, Byeong-Hyeok Sohn, "Supracolloidal polymer chains of diblock copolymer micelles", *Chem. Commun.***2014**, DOI: 10.1039/c4cc09518a.

[2] **Jeong-Hee Kim**, Su Hak Bae, Seungyong Chae, Byeong-Hyeok Sohn, "Inversion of diblock copolymer micelles by selective solvents for conversion of gold nanopatterns", *Thin Solid Films* **2012**, *520*, 2022.

[3] Thomas Basché, Klaus Müllen, **Jeong-Hee Kim**, Byeong-Hyeok Sohn, Prem Prabhakaran, Kwang-Sup Lee, "Energy and charge transfer in nanoscale hybrid materials", *Macromol. Rapid. Commun.* **2015**, submitted.

[4] Sung-Soo Kim, Myungjin Park, **Jeong-Hee Kim**, Byung Hee Hong, Byeong-Hyeok Sohn, "Wafer-scale nanoperforation of single-layer graphene by arrayed Pt nanoparticles", *Nat. Nanotechnol.* **2014**, submitted.

[5] Seungyong Chae, **Jeong-Hee Kim**, Patrick Theato, Rudolf Zentel, Byeong-Hyeok Sohn, "Dual Functionalization of Nanostructures of Block Copolymers with Quantum Dots and Organic Fluorophores", *Macromol. Chem. Phys.* **2014**, *215*, 654.

[6] Ki-Se Kim, Hun Kim, **Jeong-Hee Kim**, Jin-Hyung Kim, Chang-Lyoul Lee, Frédéric Laquai, Seong Il Yoo, Byeong-Hyeok Sohn, "Correlation of micellar

structures with surface-plasmon-coupled fluorescence in a strategy for fluorescence enhancement", *J. Mater. Chem.* **2012**, *22*, 24727.

[7] Ki-Se Kim, **Jeong-Hee Kim**, Hun Kim, Frédéric Laquai, Eric Arifin, Jin-Kyu Lee, Seong Il Yoo, Byeong-Hyeok Sohn, "Switching Off FRET in the Hybrid Assemblies of Diblock Copolymer Micelles, Quantum Dots, and Dyes by Plasmonic Nanoparticles", *ACS Nano* **2012**, *6*, 5051.

Presentations

<International>

[1] **Jeong-Hee Kim**, Jin-Hyung Kim, Myeong-Seok Seo, Byeong-Hyeok Sohn, "Combination of diblock copolymer micelles and metal nanoparticles for controlled plasmonic coupling", *Material Research Society Spring Meeting*, **2014**, San Francisco, CA, USA.

[2] **Jeong-Hee Kim**, Jin-Hyung Kim, Byeong-Hyeok Sohn, "Optoelectronic nanoparticles and nanostructures with self-assembled templates of polymeric micelles and thin films", *Material Research Society Spring Meeting*, **2012**, San Francisco, CA, USA.

[3] **Jeong-Hee Kim**, Ki-Se Kim, Byeong-Hyeok Sohn, "Controlled Fluorescence of Organic Dyes by Coupling with Hexagonal Arrays of Gold Nanoparticles", *International Research Training Group Symposium*, **2010**, Mainz, Germany.

[4] **Jeong-Hee Kim**, Ki-Se Kim, Jin-Hyung Kim, Byeong-Hyeok Sohn, "Hexagonal arrays of gold nanoparticles by block copolymer micelles for the control of coupling between surface plasmon and fluorescence", *Material Research Society Fall Meeting*, **2009**, Boston, MA, USA.

<Domestic>

[1] **Jeong-Hee Kim**, Jin-Hyung Kim, Myeong-Seok Seo, Byeong-Hyeok Sohn, "Fluorescent block copolymer micelles on plasmonic metal nanoparticles for controlled photonic coupling", *The Polymer Society of Korea*, **2014**, Daejeon.

[2] **Jeong-Hee Kim**, Hwan Kim, Jin-Hyung Kim, Byeong-Hyeok Sohn, "Mesoporous TiO2 thin films by combination of self-assembled block copolymers and nanoparticles for photovoltaic applications", *The Polymer Society of Korea*, **2012**, Changwon.

[3] **Jeong-Hee Kim**, Jae-Joon Chang, Ki-Se Kim, Byeong-Hyeok Sohn, "Fabrication of Hexagonal Arrays of Gold Nanoparticles by Block Copolymer Micelles as a Platform to Contol Surface-Plasmon-Coupled Fluorescence", *12th SNU and Hokkaido University Joint Symposium*, **2009**, Seoul.

[4] **Jeong-Hee Kim**, Jae-Joon Chang, Ki-Se Kim, Byeong-Hyeok Sohn, "Fabrication of a highly-ordered array of gold nanoparticles by block copolymer micelles for a substrate of surface-plasmon enhanced fluorescence", *The Polymer Society of Korea*, **2009**, Daejeon.